Neurobiology of Disease 130 (2019) 104536

Contents lists available at ScienceDirect

Neurobiology of Disease

journal homepage: www.elsevier.com/locate/ynbdi

Review

Visceral adiposity links cerebrovascular dysfunction to cognitive impairment in middle-aged mice

Olivier Pétrault[a,b,1], Maud Pétrault[a,1], Thavarak Ouk[a], Régis Bordet[a], Vincent Bérézowski[a,b], Michèle Bastide[a,*]

[a] Univ Lille, INSERM, CHU Lille, U1171 – Degenerative and vascular cognitive disorders, F-59000 Lille, France
[b] Univ. Artois, F-62300 Lens, France

A B S T R A C T

Midlife cognitive decline is now recognized as a factor of poor prognosis for late-life dementia. Although an epidemiological link has been suggested with high fat diet (HFD)-induced metabolic disorders, the effect of a long period of HFD on midlife cerebrovascular and cognitive functions remains unproven. A cohort of 216 young mice was fed with HFD up to middle age (12 months), and kinetically characterized for metabolic status, including weight, blood lipid profile, hepatic fat accumulation, glucose intolerance, and visceral adiposity. Metabolic disorders were evidenced from 3 months of HFD. Visual recognition memory and flexibility were significantly altered and associated to a visceral adiposity whereas spatial reference memory and working memory did not. Concomitantly, a progressive dysfunction of the vascular endothelium-dependent relaxation was detected in both middle cerebral artery and parenchymal arterioles, with consequences on the regulation of cerebral blood flow, but without any modification of the basal brain tissue MRI perfusion signal. Our data collection empowered us to stratify the mice according to their heterogeneous response to diet, and to propose a statistical prediction model for cognitive impairment, combining visceral adiposity and cerebral vasomotion in a diagnostic perspective of early neurological deficits.

1. Introduction

Cognitive decline is an age-related decrease in cognitive functions. Initially slow and progressive, cognitive decline can be enhanced by various risk factors and events, potentially leading to dementia. Dementia includes ability loss as well as changes in behavior, and is defined as a global, durable and organic alteration of mental health, which hinders the individuals' autonomy in everyday life, leading to dependency. Therefore, dementia is recognized as the greatest global challenge for health in this century (Livingston et al., 2017). The presence of a premature cognitive decline is now accepted as a factor of poor prognosis for late-life dementia (Kivipelto et al., 2006; Vuoksimaa et al., 2016). Its onset around the middle-age period does not often lead to a cognitive complaint, and implies a potential input of high fat diet (HFD)-induced metabolic disorders (Debette, 2013; González et al., 2018; Lourenco et al., 2018; Whitmer et al., 2005). Indeed, these disorders include a constellation of elements ranging from imbalanced metabolism to an acute cardiovascular or cerebrovascular event, the latter being the only well-known precipitating factor for late-life dementia. Anyhow, cerebral vessels are spotlighted as a first line interface between blood lipids and brain, but apart from stroke, the effect of a long period of HFD on midlife cerebrovascular and cognitive functions remains unproven, because of the influence of the multiple factors accounting for the diversity of human life styles (Livingston et al., 2017; van Dijk et al., 2015).

Therefore, evidencing such an effect would define diet as a modifiable risk factor for mental health, and help identify, among dyslipidemic patients, those at risk of cognitive decline. Such a demonstration needs however a long-term investigation, with few confounding factors, but including the variety of responses to diet. Several studies have checked the involvement of neuroinflammatory and oxidative mechanisms (Francis and Stevenson, 2013; Pistell et al., 2010; Sabia et al., 2009; Wang et al., 2016) as well as alterations of peripheral vasculature (Costa et al., 2018; Tesauro and Cardillo, 2011), but nothing was found about their influence on cerebrovascular function. And yet, cerebral vessels have unique features and are tightly associated to the brain tissue. A long-term exposure to metabolic disorders could impair the function of different segments of the vascular tree, i.e. external cerebral arteries, parenchymal arterioles or capillaries, and lead to brain hypoperfusion (Haley et al., 2017), possibly affecting cognition at midlife.

To test the effect of HFD on cognition, we have induced progressive metabolic disturbances in young adult wild type mice (8 weeks) with a

* Corresponding author at: Laboratoire de Pharmacologie U1171, Faculté de Médecine, 1 place de Verdun, F-59045 Lille cedex, France.
E-mail address: michele.bastide@univ-lille.fr (M. Bastide).
[1] Both authors contribute equally to this study.

https://doi.org/10.1016/j.nbd.2019.104536
Received 18 February 2019; Received in revised form 7 June 2019; Accepted 15 July 2019
Available online 17 July 2019

40% *w/w* animal fat-enriched diet up to the middle age (12 months later), and kinetically (every 3 month) assessed spontaneous locomotor, and cognitive functions. To cope with potential heterogeneity of the responses to diet and to long-term follow up, we have set up a cohort of 216 mice and fully characterized their metabolic status. These mice were then challenged for the vasomotor function of their middle cerebral arteries (Halpern arteriography) and parenchymal microvessels (*in situ* brain slices), for brain perfusion (ASL MRI perfusion) and cerebral blood flow (Doppler laser). The modified metabolic, cerebrovascular, and cognitive data were correlated and tested for their diagnostic potential through a statistical extrapolation model.

2. Materials and methods

2.1. Animals diets and cohorts

All procedures were performed in accordance to the European Directive (2010/63UE) and were approved by the local animal care and use (Comité d'Ethique en Expérimentation Animale du Nord-Pas-de-Calais, Lille, France, reference: APAFIS#4624–20-16030215325945 v5). Two hundred and sixteen adult male C57Bl6/J mice, reported in different cohorts (n = 12 cohorts), aged of 8 weeks at the onset of the study (Janvier Labs, Le Genest Saint Isle, France) were housed in standard cage. At the start of the experiment, mice were randomly assigned to either a nutritionally complete, high-fat diet (HFD) consisting of 40% saturated fat, mostly from lard (HF231, Safe, Augy, France) or a control diet (ND) consisting of 3% fat (A04, Safe, Augy, France) throughout the experimental period (Table 1). All animals had *ad libitum* access to food and water. Seven unexpected death occurred during the study, bringing ND group to n = 100 mice and HFD group to n = 109 mice in total. There were no significant differences in body weight between groups before the experimental diets were administered, as mice had been maintained on a regular chow diet. The animals were weighed every month. At the following time-points: 0, 3, 6, 9 and 12 months of ND or HF diet, mice were undergoing battery of behavioral tests and MRI and some of them were sacrificed *via* the intraperitoneal administration of a lethal dose of sodium pentobarbital (182 $mg.kg^{-1}$) to perform brain vascular analysis (Appendix Fig. A.1).

2.2. Metabolic characterization

2.2.1. Blood triglycerides and cholesterol assays

At the different time-points, mice were fasted overnight and anesthetized with 2% isoflurane to collect blood samples at the retro-orbital sinus. Total cholesterol (TC), nonHDL cholesterol, HDL cholesterol and triglycerides plasma concentrations were determined by enzymatic colorimetric assays using commercially available kits (Thermofisher Scientific, Illkirch, France).

2.2.2. Oral glucose tolerance test

After an overnight fasting, plasma glucose levels were determined with glucometer system Accu-Chek® Performa (Roche Diagnostic, Mannheim, Germany) on a blood sample collected from the mouse tail vein. Then, they received orally 2 g/kg body weight of D-glucose. Ten, 20, 30, 60, 90 and 120 min after, glucose quantification was performed. Area under the curve (AUC) was calculated using GraphPad Prism 5, (GraphPad Software Inc., La Jolla CA, USA).

2.2.3. Visceral adipose tissue weight

After sacrifice, adipose tissue from perirenal and epididymal depots was collected and weighted.

2.2.4. Steatosis

After sacrifice, liver is collected and biopsies realized. They are fixed with 4% paraformaldehyde, dehydrated, embedded in a matrix (OCT®). Biopsies are frozen in liquid N_2 and subjected to frozen sectioning. Oil red O (ORO) staining was performed to detect neutral lipids. The frozen tissue sections (8-µm thickness) were immersed in 0.5% oil red O working solution for 15 min, counterstained with hematoxylin, and then rinsed under running tap water for 10 min. Photomicrographs were captured under a microscope (DMR Leica DMLB, Germany) from different views. The integrated optical density (IOD) of the oil red O-stained area was analyzed with ImageJ freeware. The evaluator was blinded to the diet status of the evaluated samples (3 to 6 animals per group, from 3 independent experiments).

2.3. Behavioural assessments in the mouse

At the following time-points: 0, 3, 6, 9 and 12 months of ND or HF diets, mice of each group underwent a battery of test evaluating spontaneous motor activity (actimetry), spatial reference memory and flexibility (Barnes test), visual recognition memory (novel object recognition test) and working memory (spontaneous alternation test). The mice were tested between 9 a.m. and 2 p.m. During the experiments, the equipment was cleaned with 70% ethanol after each trial so that olfactory cues did not bias the results.

2.3.1. Spontaneous motor behaviour

Spontaneous motor activity was measured in an actimeter (Panlab, Bioseb, Vitrolles, France). The test apparatus (a 45 cm in length × 45 cm in width × 35 cm in height, transparent polymethylmethacrylate chamber with a black floor) was equipped with

Table 1
Nutrient and energy profiles of normal diet (ND) and high fat diet (HFD).

	Nutrients (%)	Energy (%)	Energy (kcal/kg)	Nutrients (%)	Energy (%)	Energy (kcal/kg)
	ND			HFD		
Proteins	16.2	19.3	648	28.7	21.3	1148
Lipids	3.2	8.4	288	40.1	70.7	3620.2
Carbohydrates	60.5	72.3	2420	14.2	8	567.6
Minerals	4.6			8.2		
Cellulose	3.9			3.1		
Humidity	11.6			5.6		
	100	100	3326	100	100	5335.8

two infrared sensor frames, so that horizontal displacements could be measured. Motor activity (beam obstruction) was recorded for 10 min, using a computer. To diminish odour cues, the chamber's floor was covered with sawdust. Total distance covered (in cm), and the resting time (in seconds) were quantified for each mouse (Marche et al., 2011).

2.3.2. Spontaneous alternation

The spontaneous alternation test was performed using a Y-maze (made of white polyvinyl chloride) and a closed-circuit video camera (Ethovision XT, Noldus, Wageningen, The Netherlands). The three arms were of the same size (30 × 8 × 15 cm) and were oriented at an angle of 120° to each other. The Y-maze was placed in a room with no environmental cues. The mouse was placed at the end of one arm and was allowed to move freely between the maze's three arms for 8 min. A visit to an arm was scored when all four of the mouse's paws were within the arm area. The sequence of the arm visits was recorded, and an alternation response was scored when the animal entered the least recently visited arm. The alternation score was calculated as the ratio between actual alternations and possible alternations (defined as the total number of arm visits minus 2), multiplied by 100 (Hidaka et al., 2008). This calculation was only performed for mice making more than twenty arm visits.

2.3.3. Barnes maze

The Barnes maze test of learning, and spatial reference memory and cognitive flexibility was performed on two following weeks essentially as described by Sunyer et al. (Sunyer et al., 2007). The apparatus consisted of a circular white PVC platform (diameter: 122 cm) positioned 80 cm above the ground. Forty holes (diameter: 5 cm) were located at regular intervals 4 cm from the edge. Spatial cues were placed on the walls of the testing room and were not moved at any point during the study period. An aversive bright light (800 Lux) was used as a stimulus to motivate the mice to find a single black escape box (22.9 × 5.3 × 8.6 cm) located beneath one of the holes. The circular platform was virtually divided in eight zones including the target quadrant (including the target quadrant with the escape box and the opposite quadrant). One of forty possible escape hole (i.e. the target hole) was randomly assigned to each mouse for all five days of the experiment.

2.3.3.1. First week. During the acquisition phase (4 trials per day for 4 days with a 15-min break between trials), the mouse was placed at the center of the maze in an opaque cylinder for 10 s and then left to freely explore the maze and search for the escape box for up to 3 min. Once the mouse had entered the escape box, it was left there for 1 min. The location of the target was consistent for a given mouse but randomized across mice. On the fifth day (for the probe trial), the maze was turned by 45, and the escape box was removed. The mouse was allowed to move freely for 90 s. A video camera and a computer running Ethovision XT 11.5 software (Noldus) were used to track and to analyze the animal's displacements during the session. The number of total errors (the number of holes visited before the mouse enter in the target hole) were noted as the indices of learning during the acquisition phase. Spatial reference memory was evaluated as the time spent in the target quadrant (i.e. the quadrant centered on the target hole) and in the opposite quadrant during the probe trial.

2.3.3.2. Second week. For two days after the memory retention trials, mice were tested for reversal learning. The same acquisition training was used as previously described but the location of the escape box for each mouse was shifted 180°. Each day during the 3 days' learning consisted of four trials. On the test day, the time the mouse spent in the target quadrant and in the opposite quadrant was measured to evaluate the cognitive flexibility.

2.3.4. Novel object recognition test

The novel object recognition test is based on the tendency of mice to explore a novel object rather than a familiar one. Mice were habituated to a square arena (50 × 50 × 25 cm) for 10 min on the first day. On day 2, the mice were exposed to the arena containing two identical objects (two cylindrical glasswares, Ø: 4 cm, height: 6 cm). On day 3, mice were exposed in a first phase ("sample phase") to two novel and identical objects (either a Lego®square structure 4x4x6 cm or a golf ball with a blue cap Ø: 4 cm, height: 6 cm) for 15 min and then returned in their cages. After one hour, they are placed back in the testing arena for 5 min ("test phase"), but one of the familiar objects was replaced by a novel object. Performance of the mice was video recorded (Ethovision XT, Noldus, Wageningen, The Netherlands). The objects had been previously validated to ensure there was no inherent preference for either object (data not shown). Exploratory behaviour was defined as the animal directing its nose towards the object at a distance < 2 cm. Any subjects that failed to complete a minimum of 20 s of exploration during the sample phase were excluded from the analysis. A discrimination index was calculated as the difference between the time spent exploring the novel object minus the time spent exploring the familiar object divided by the sum of both (Antunes and Biala, 2012).

2.4. In vivo MRI acquisition and processing

All MRI experiments were performed on a Biospec 7.0 T/20 cm horizontal magnet (Bruker, Ettlingen). Animals were first anesthetized with isoflurane and then placed in a dual-coil small animal restrainer which contains a volume coil for transmitting and a surface quadratic coil for receiving. Coil-to-coil electromagnetic interaction was actively decoupled. Blood gases saturation and respiration rates of animals were continuously monitored *via* specific transducers. Their rectal temperature was monitored and maintained at 37 ± 1 °C *via* a feedback-regulated circulating water pad (SA Instruments Inc. Stony Brook, NY USA).

Anatomical images were acquired using the fast spin echo rapid acquisition relaxation enhanced (RARE) pulse sequence with TR = 2500 ms, effective TE = 33 ms, matrix: 256 × 256, FOV = 2 × 2 cm, twenty 0.5- mm slices, and 2 averages. The sequence of diffusion-weighted image (DWI) was performed in three directions [1, 0, 0], [0, 1, 0], [0, 0, 1] for which 11 b-values were used to characterize signal decay. The b-values were defined as follows: 1, 10, 20, 30, 40, 60, 80, 100, 400, 600, 800, and 1000 s/mm^2. The sequence parameters were as follows: FOV = 2 × 2 cm; matrix size: 128 × 128; slice thickness = 1 mm; TR = 3000 ms; TE = 33 ms. Parametric ADC maps were constructed using paravision 5.1 software (Bruker). Fluid-attenuated inversion and recovery (FLAIR) images were acquired in the coronal plan from optimized RARE pulse sequence with TR = 5000 ms, TE = 33 ms and TI = 1600 ms (inversion), FOV = 1.5 × 1.5 cm, matrix size: 150 × 150. The gradient echo sequence with specific parameters TR = 350 ms, TE = 18 ms, FA = 40°, FOV = 1.5 × 1.5 cm, matrix size: 372 × 372, was used to assess the magnetic susceptibility of brain tissue. Arterial spin labelling (ASL) perfusion quantifications were acquired using the echo-planar imaging (EPI) and flip angle inversion and recovery (FAIR) pulse sequence with TR = 18,000 ms, effective TE = 13.5 ms, FA = 90° and TI = 26 ms with 30 increments of 150 ms. The principle of ASL perfusion quantification is based on the difference between background static spins (global MR signal of brain) and blood non-static spins magnetically "labelled" (spin inversion upstream). The

signal of specific spin recovery of blood characterizes the blood supply speed and can be used to quantify brain perfusion.

2.5. Cerebrals vessels study

2.5.1. Determination of cerebral blood flow by laser-doppler flowmetry

Mice were anesthetized with 2%isoflurane. They were immobilized and placed in a stereotaxic frame (David Kopf Instruments). The scalp and the periosteum were pulled aside. The rectal temperature was maintained at 37 °C using a thermostatic heating pad (Panlab, Bioseb, Vitrolles, France). A laser Doppler probe (Perimed, Periflux System, Stockolm, Sweden) was positioned above the left MCA territory (-0.1 to 1.10 mm rostro-caudal and 2–3 mm lateral to bregma).

2.5.2. Ex vivo middle cerebral artery reactivity analysis

At Day 0, 3, 6, 9 and 12 months after diet and after anesthesia with sodium pentobarbital (182 $mg.kg^{-1}$), brain was removed and the MCA was dissected. *Ex vivo* vasoreactivity was assessed in a Halpern arteriograph (Living System Instrumentation, Burlington, USA) on a proximal segment of the right MCA, perfused with an oxygenated Krebs solution (in mM): 119 NaCl, 24 $NaHCO_3$, 4.7 KCl, 1.18 KH_2PO_4, 1.17 $MgSO_4$, $7H_2O$, 10 glucose, 1.6 $CaCl_2$, pH = 7.4) kept at 37 °C. The artery was secured to the proximal and distal cannulae with nylon ties. The distal cannula was closed in order to work under "no flow" conditions. The arteriograph chamber was continuously supplied with Krebs solution equilibrated with 20% O_2/5% CO_2/balance N_2. The proximal cannula was connected to a pressure transducer, a miniature peristaltic pump and a servo-controller that continually measured and adjusted transmural pressure. The entire arteriograph system was positioned on the stage of an inverted microscope equipped with a video camera and a display monitor. The lumen diameter was measured by video image dimension analysis. The artery segment was left to stabilize for 1 h at an intraluminal pressure of 20 mmHg. The maximal constriction of the artery was tested with phenylephrine (Phe) 30 μM. To evaluate endothelium-dependent relaxation, the maximal response to carbachol (Carb) 10 μM was determined after preconstriction with Phe 30 μM. For constriction, results are expressed as % maximal constriction using the following equation: % maximal constriction = (Diameter $_{basal}$ − Diameter $_{Phe}$)/(Diameter $_{basal}$) × 100. For endothelium-dependent relaxation, results are expressed as % increase compared with the preconstricted artery diameter using the following equation: % maximal relaxation = (Diameter $_{Carb}$ − Diameter $_{Phe}$)/(Diameter $_{basal}$ − Diameter $_{Phe}$) × 100.

2.5.3. Ex vivo brain slice model

At Day 0, 3, 6, 9 and 12 months after diet, brain were removed from selected mice after anesthesia with sodium pentobarbital and put in a chamber containing ice-cold solution of aCSF (in mM: 124 NaCl, 3.5 KCl, 2 $MgSO_4$, 1.25 NaH_2PO_4, $2CaCl_2$, 26 $NaHCO_3$, 11 glucose, pH 7.4) continuously bubbled with carbogen (95% O_2–5% CO_2). Coronal cortical and hippocampal slices (250–300 μm) were cut on a vibratome (World Precision Instruments, Stevenage, UK) and subsequently laid on mesh submerged in an aCSF recovery chamber at room temperature. Slices received continuous bubbling of carbogen and recovered for 60 min. Brain slices were transferred to a perfusion chamber (Warner Instruments, Harvard Apparatus, Les Ulis, France). Blood vessels were visualized with an upright Leica DMLFS microscope equipped with differential interference contrast (DIC) and a CCD camera (COHU, Pieper GmbH, Düsseldorf, Germany). We selected vessels showed structures reminiscent of vascular myocytes, had a discernible luminal diameter of 7 ± 3 μm and could be controlled for their integrity for a length of 100–150 μm. Images of vascular responses were acquired with image software (Magix Video Terratec Edition, Berlin, Germany). To measure the diameter, we compared off-lines images acquired at the same focal plane from 1 to 4 sectors. Intraluminal diameters for each experimental condition were obtained as an average of 2 measurements taken. In the different experiments, the number of arterioles studied corresponds to the number of slices used (only one arteriole per slice was examined). Imaging was performed at 20–22 °C and perfused at 7 mL/min.

2.5.4. Microvascular patency and blood-brain barrier integrity

The fluorescence-based visualization of brain microvascular patency as well as blood brain barrier integrity was enabled by the observation of both distribution and extravasation of fluoresceinisothiocyanate (FITC)-Dextran (2000 kDa, 10 $mg.mL^{-1}$, Sigma-Aldrich, Saint-Quentin Fallavier, France) through patent microvessels. A 100 μL volume of FITC-Dextran in physiologic saline solution was injected into the penis vein of mice. After 2 min, mice were decapitated. Brains were extracted and post-fixed in 4% paraformaldehyde for 24 h at 4 °C, embedded in OCT compound, and frozen in liquid nitrogen. Forty micrometer-slices were coronally cut using a cryostat, and mounted with Vectashield hardset medium with DAPI (Vector Laboratories, Burlingame, CA, USA). Because of the important tortuosity of brain microvessels, slices were visualized under an automated microscope (AxioScan digital slide scanner, Zeiss microscopy, Marly le Roi, France) enabling a z-stack projection of the scanned sections, to obtain a focused image of microvascular segments. The evaluator was blinded to the diet status of the evaluated samples (3 to 6 animals per group, from 3 independent experiments).

2.6. Neuropathological analysis

Three, six, nine and twelve months after diet, brain were removed from selected mice, fixed in methacarn for 24 h and embedded in paraffin. Five-micrometer slices were coronally cut, stained with haematoxylin/eosin, and observed under a bright-field microscope. Neuropathological lesions (tissue loss or abnormal organization, microbleeds or other vascular alteration) were seeked throughout the whole brain sections. Only those from the prefrontal cortex and hippocampus areas are presented in figures, since accounting for the neurological deficits observed after the behavioral assessments. The evaluator was blinded to the diet status of the evaluated samples (3 to 6 animals per group, from 3 independent experiments).

2.7. Drugs

All vasoactive drugs, phenylephrine, sodium nitroprusside (SNP), carbachol, endothelin-1 (Sigma-Aldrich, St Quentin-Fallavier, France) were made fresh daily and stored at 4 °C.

2.8. Statistical analysis

All values were expressed as mean ± standard error of the mean (SEM). Statistical analyses were performed using R software version 3.4.0 (R Core Team (2017) R: A language and environment for statistical computing. R Foundation for Statistical Computing, Vienna, Austria.URL https://www.R-project.org/), and R Studio environment version 1.0.143. Multiple inter-group differences were tested for the nature of the diet and its duration by a 2-way ANOVA (*Diet* × *Time*) and independently for the weight categories by a 1-way ANOVA followed by, where appropriate, a post-hoc tests based on Tukey's 'Honest

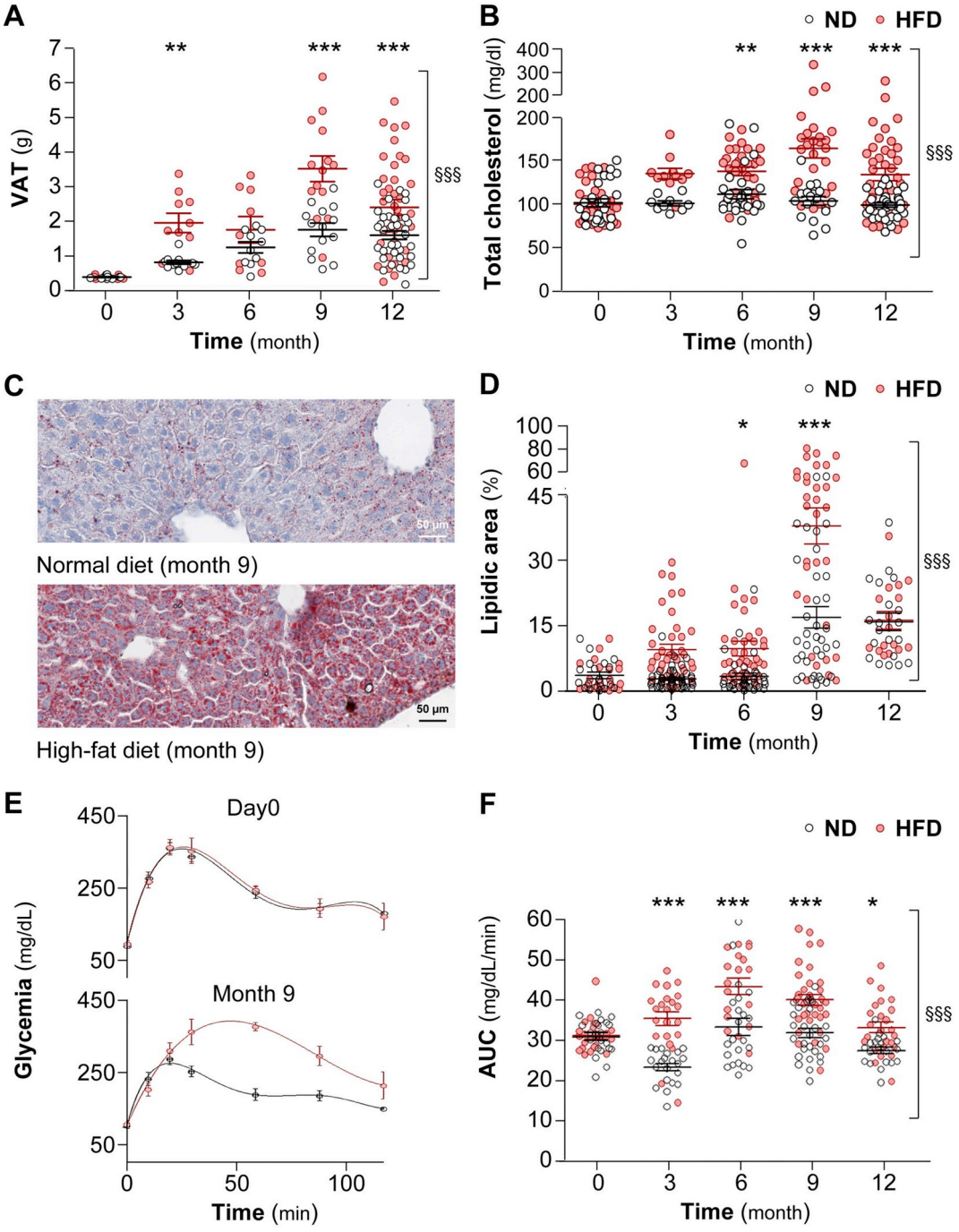

Fig. 1. Changes in lipid and glycemic parameters in normal diet (ND)-fed mice and high fat diet (HFD)-fed mice from Day0 up to 12 months. (A) Changes in visceral adipose tissue weight (VAT in g) dissected from ND (n = 77) mice and HFD (n = 80) mice. (B) Total cholesterol (mg/dL) assayed in plasma from ND (n = 100) mice and HFD (n = 109) mice. (C) Liver lipid infiltration in ND and HFD mice stained by Oil Red O staining (x20). Representative illustrations of serial liver sections from a ND mouse and a HFD mouse after 9 months of diet. (D) Quantification of lipid accumulation in livers from ND (n = 156) and HFD (n = 148) mice at different diet time-points. (E) Glucose intolerance has been tested with an oral glucose tolerance test (OGTT). Representative kinetics of glycemia values obtained from ND mice and HFD mice have been illustrated at Day0 and M9. (F) Area under the curve (AUC) quantifications for OGTT of ND (n = 100) and HFD (n = 109) mice at the different time-points.

Data are shown as mean ± sem with points of individual measurements. Statistical analysis was performed using a two-way ANOVA, $^{§§§}p < .001$ for the effect of the *Diet* factor. Tukey *post hoc* analysis was performed: *p < .05, **p < .01, ***p < .001 for HFD *vs* ND comparison.

Significant Difference' adjustment method. Variance analyses were assessed using "ez" package version 4.4-0 (Michael A. Lawrence (2016) ez: Easy Analysis and Visualization of Factorial Experiments. R package version 4.4-0. https://CRAN.R-project.org/package=ez). Proportions of weight categories were compared using Pearson's chi-squared test. The *a posteriori* calculation of Pearson's correlation coefficient (r) or Kendall's rank correlation (tau) was systematically followed by the power calculation using "pwr" package (Stephane Champely (2018) pwr: Basic Functions for Power Analysis. R package version 1.2-2. https://CRAN.R-project.org/package=pwr). The extrapolation model was generated from normalized values for our datasets following the next equation: y = 100/(1 + 10^(x-f50%) where y = Normalized vascular or cognitive function (%); x = VAT (g) and f50% = the VAT fitted value at half of the function (g). The threshold for statistical significance was set to $p < 0.05$.

3. Results

3.1. Diet induces heterogeneous weight gain and metabolic disturbances

The metabolic status of each mouse was characterized at each time-point (D0, M3, M6, M9 and M12) of diet duration. Multiple comparisons between normal diet (ND) and high-fat diet (HFD) mice were also tested at each time-point by 2-way ANOVA (Time: diet duration; Diet: type of diet) for metabolic parameters such as adipose tissue deposition, circulating plasma lipids, liver fat accumulation, glucose tolerance (Fig. 1 and Table 2), and weight (Fig. 2).

In HFD-fed mice, a significant increase was found in visceral adipose tissue deposition with a major statistical contribution of Diet ($F_{1,140} = 36.50$, $p < 0.001$, Fig. 1A). HFD induced an increase in plasma total cholesterol level (major contribution of Diet: $F_{1,227} = 48.35$, $p < 0.001$, Fig. 1B) as well as in non-HDL cholesterol and in HDL cholesterol levels (Table 2A).

Histological analysis of the liver revealed a more prominent Oil Red O (ORO) stain in HFD-fed mice as illustrated in Fig. 1C and quantified in Fig. 1D. This difference reached statistical significance after 6 months, but was more obvious after 9 months of HFD, and then fell down to the same level as that of ND-fed mice at 12 months. There was a significant effect of Time ($F_{4,294} = 50.99$, $p < 0.001$) and Diet ($F_{1,294} = 26.43$, $p < 0.001$).

Fasting glycemia was not different between ND- and HFD-fed mice whatever the diet duration (Table 2A). The Oral Glucose Tolerance Test (OGTT) showed superimposed curves at day 0 while after 9 months of diet, the time to glycemic peak in HFD-fed mice was delayed from 20 to 50 min, reached a higher value and failed to drop as fast as in ND-fed mice (Fig. 1E). These variations were confirmed by the plot of Area Under the Curve (AUC, Fig. 1F). A major significant effect of Diet was found ($F_{1,177} = 64.61$, $p < 0.001$).

A weight gain was observed, with a significant contribution of both Time ($F_{4,753} = 390.95$, $p < 0.001$) and Diet ($F_{1,753} = 50.14$, $p < 0.001$). In both diet populations, weight gain was not homogeneous all over the study period (Fig. 2A, dots in scatter plot). Post-hoc multiple comparisons revealed greater weight differences between ND- and HFD-fed mice after 3, 6 and 9 months but not after 12 months of diet (Fig. 2A). As no standard values exist for the definition of weight categories in mice, we suggest building three weight categories from our results. We used a linear statistical model of the relation between weight gain and visceral fat deposition to deduce the weight value for which fat deposition was doubled. In our cohort, ND-fed mice developed a maximum of 2 g of visceral adipose tissue ($ND_{mean+sd}$: 1.37 + 0.63 g). Therefore, we calculated the fitted weight values for 2 g and 4 g of visceral adipose tissue and found 36.1 g and 43.7 g respectively. Mice were then considered as of normal weight (> 20 g to 36.1 g), overweight (> 36.1 g to 43.7 g) or obese (> 43.7 g) (Fig. 2B). These weight categories were further used in a secondary analysis of each result of the study. For instance, HFD has clearly modified the

Table 2
Metabolic parameters assayed on ND and HFD-fed mice at different time-points (A) on weight-categorized mice (B).

A: *vs Time* and *Diet*		D0	M3	M6	M9	M12
Visceral adipose tissue (g)	ND	0.36 ± 0.02 (5)	0.80 ± 0.05 (12)	1.24 ± 0.16 (10)	1.75 ± 0.20 (14)	1.60 ± 0.12 (36)
	HFD	0.38 ± 0.01 (5)	1.96 ± 0.28 (10)	1.76 ± 0.39 (9)	3.54 ± 0.38 (14)	2.34 ± 0.23 (35)
Triglycerides ($mg.dL^{-1}$)	ND	103.7 ± 5.6 (27)	138.2 ± 15.9 (10)	111.6 ± 13.0 (18)	98.0 ± 7.3 (21)	97.0 ± 5.3 (34)
	HFD	116.2 ± 6.4 (32)	150.8 ± 8.3 (11)	131.9 ± 9.1 (20)	111.4 ± 5.7 (24)	103.7 ± 5.2 (36)
Total cholesterol ($mg.dL^{-1}$)	ND	101.0 ± 4.5 (27)	100.4 ± 2.9 (10)	110.7 ± 5.3 (18)	103.1 ± 5.0 (21)	98.8 ± 2.4 (34)
	HFD	99.52 ± 3.7 (32)	134.0 ± 6.0 (11)	136.7 ± 4.8 (20)**	162.5 ± 10.8 (24)***	133.0 ± 7.1 (36)***
HDL cholesterol ($mg.dL^{-1}$)	ND	60.8 ± 3.2 (27)	65.7 ± 4.8 (10)	67.4 ± 3.1 (18)	68.5 ± 4.9 (21)	64.8 ± 2.5 (34)
	HFD	60.9 ± 3.1 (32)	90.1 ± 4.8 (11)	82.4 ± 5.2 (20)	103.6 ± 10.2 (24)***	81.4 ± 6.9 (35)
NonHDL cholesterol ($mg.dL^{-1}$)	ND	40.24 ± 2.2 (27)	34.25 ± 5.4 (10)	32.9 ± 3.1 (18)	34.7 ± 3.0 (21)	32.8 ± 1.8 (34)
	HFD	38.7 ± 1.5 (32)	44.0 ± 2.8 (11)	51.8 ± 3.0 (20)***	58.9 ± 3.6 (24)***	52.1 ± 2.2 (35)***
Fasting glycemia ($mg.dL^{-1}$)	ND	85.0 ± 2.8 (15)	94.29 ± 1.6 (21)	103.3 ± 4.2 (17)	106.1 ± 3.9 (12)	89.5 ± 2.5 (20)
	HFD	91.3 ± 2.3 (15)	96.6 ± 4.3 (22)	121.0 ± 8.3 (26)	118.4 ± 7.3 (12)	102.4 ± 3.3 (24)
OGTT (AUC, $mg.min.dL^{-1}$)	ND	29,070 ± 1055 (15)	22,951 ± 891 (21)	31,670 ± 2828 (16)	32,202 ± 2115 (12)	27,004 ± 791 (20)
	HFD	29,499 ± 656 (15)	35,307 ± 1659 (23)***	42,847 ± 2093 (26)***	37,511 ± 1575 (12)***	32,732 ± 1356 (23)*

B:*vs* weight categories	Normal weight	Overweight	Obese
Visceral adipose tissue (g)	1.16 ± 0.07 (90)	2.67 ± 0.14 (48)***	3.85 ± 0.43 (12)***
Triglycerides ($mg.dL^{-1}$)	120.4 ± 3.5 (159)	124.1 ± 6.1 (59)	145.5 ± 13.3 (15)
Total cholesterol ($mg.dL^{-1}$)	106.8 ± 26 (159)	135.8 ± 40 (59)***	213.5 ± 65 (15)***
HDL cholesterol ($mg.dL^{-1}$)	68.2 ± 23 (158)	88.5 ± 32 (59)***	145.9 ± 68 (15)***
NonHDL cholesterol ($mg.dL^{-1}$)	38.5 ± 14 (158)	47.4 ± 16 (59)*	67.6 ± 12 (15)***
Fasting Glycemia ($mg.dL^{-1}$)	93.9 ± 1.5 (127)	108.4 ± 3.3 (41)***	130.6 ± 8.8 (16)***
OGTT (AUC, $mg.min.dL^{-1}$)	29,937 ± 648 (127)	35,703 ± 1558 (41)***	41,523 ± 2051 (15)***

Results are expressed in mean ± SEM. Statistical analysis was performed using a two-way ANOVA, $^{§§§}p < 0.001$, $^{§}p < 0.05$ for the effect of the *Diet* factor; one-way ANOVA $^{£££}p < 0.01$, $^{£}p < 0.05$ for the effect of the *Weight categories* factor. Tukey post hoc multiple comparisons were performed: $^{*}p < 0.05$, $^{***}p < 0.001$ for HFD *vs* ND comparison (2-way ANOVA) or *vs* Normal weight comparison (1-way ANOVA).

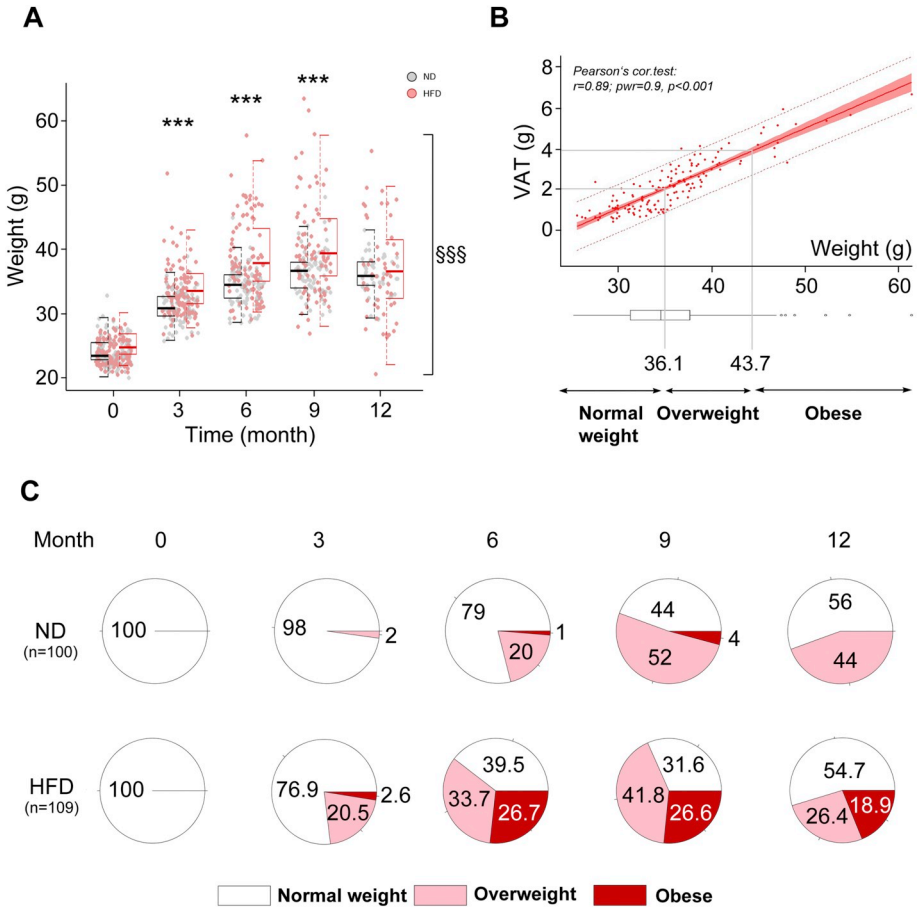

Fig. 2. Body weight in normal diet (ND)-fed mice and high fat diet (HFD)-fed mice up to 12 months of diet. (A) Kinetic and dispersion of weight in ND (grey circles) and HFD (pink circles) mice groups. (B) Stratification of mice according to linear regression between weight and visceral fat deposition over the study period. (C) Post-stratification proportions (in %) of mice according to three categories: normal weight, overweight and obese.
Statistical analysis was performed using a two-way ANOVA (*Diet* factor: $^{§§§}p < .001$). Tukey *post hoc* multiple comparisons were performed: $^{***}p < .001$ for HFD *vs* ND. Pearson's correlation test disclosed a strong significant relationship between the visceral fat deposition and weight ($r = 0.89$; $p < .001$). (For interpretation of the references to colour in this figure legend, the reader is referred to the web version of this article.)

weight gain pattern of mice (Pearson's chi-square test: Chi-square (2763) = 51.18, $p < 0.001$, Fig. 2C), especially the obese (chi-square contribution 22.06). An increasing proportion of overweight mice was noticed from 3 months, even in the ND-fed group reaching 44% at 12 months. Surprisingly, most HFD-fed mice lost weight after 12 months of diet. Indeed, 40% of mice that were obese at 9 months have lost > 10% of their weight at 12 months, and consequently changed of weight category.

When considering these weight categories, the metabolic status was redistributed, as detailed in Table 2B. For instance, mean values of blood lipid levels were significantly higher in overweight and obese mice compared to normal-weight mice, except for triglyceride levels. Fasting glycemia was significantly higher in overweight and obese mice compared to normal-weight mice (Nw: 93.9 ± 1.5 mg.dL^{-1}*vs* Ow: 108.4 ± 3.3 mg.dL^{-1} and Ob: 130.6 ± 8.8 mg;dL^{-1}, $p < 0.001$). The reduced capacity to clear glucose from blood was significant in overweight and obese mice compared to the normal-weight mice (Nw: 29937 ± 648 mg.min.dL^{-1}*vs* Ow: 35703 ± 1558 mg.min.dL^{-1} and Ob: 41523 ± 2051 mg.min.dL^{-1}, $p < 0.001$).

3.2. Specific cognitive functions are impaired by high fat diet or overweight

Whatever the diet type and duration, no difference was obtained in spontaneous locomotor activity, as reflected by the total distance travelled and the resting time (Fig. 3A and B, left panels). Regarding weight categories, a significant reduction in the travelled distance ($F_{2,232} = 8.93$, $p < 0.001$), and an increase in the resting time (chi-square(219,2) = 6.96, $p < 0.05$) were observed and associated to obese status (Fig. 3A and B, right panels).

Working memory was not impaired in HFD-fed mice compared to ND-fed mice whatever the time-point, as given by the spontaneous alternation ratio (Fig. 3C, left panel), and no significant difference was observed among weight categories (Fig. 3C, right panel). Visual recognition memory of the ND-fed mice was preserved, since evidenced by a stable discrimination index (NOR index) of around 0.37 (Fig. 3D, left panel). Conversely, the discrimination index of HFD-fed mice decreased progressively until 12 months, with a very significant effect of *Diet* ($F_{1,172} = 46.56$, $p < 0.0001$). Indeed, the ability of these mice to discriminate a novel object from a familiar one was reduced by > 70% after 12 months of HFD. Besides, the more the weight, the less the NOR index ($F_{2,179} = 11.76$, $p < 0.001$, Fig. 3D, left panel), as evidenced by a significant fall in the index between normal-weight and overweight mice ($p < 0.05$), normal-weight and obese mice ($p < 0.001$), overweight and obese mice ($p < 0.05$).

Spatial reference memory and memory flexibility were assessed in all mice using Barnes maze on two successive weeks, but only the results obtained with mice exposed to 9 months of diet are presented (Fig. 4), as the metabolic disturbances were the most important at that time point. Throughout the acquisition training period (week 1), the spatial reference memory of both ND- and HFD-fed mice was preserved (Fig. 4A, left panel), and no significant difference was observed among weight categories (Fig. 4A, right panel). As well in the probe test, the

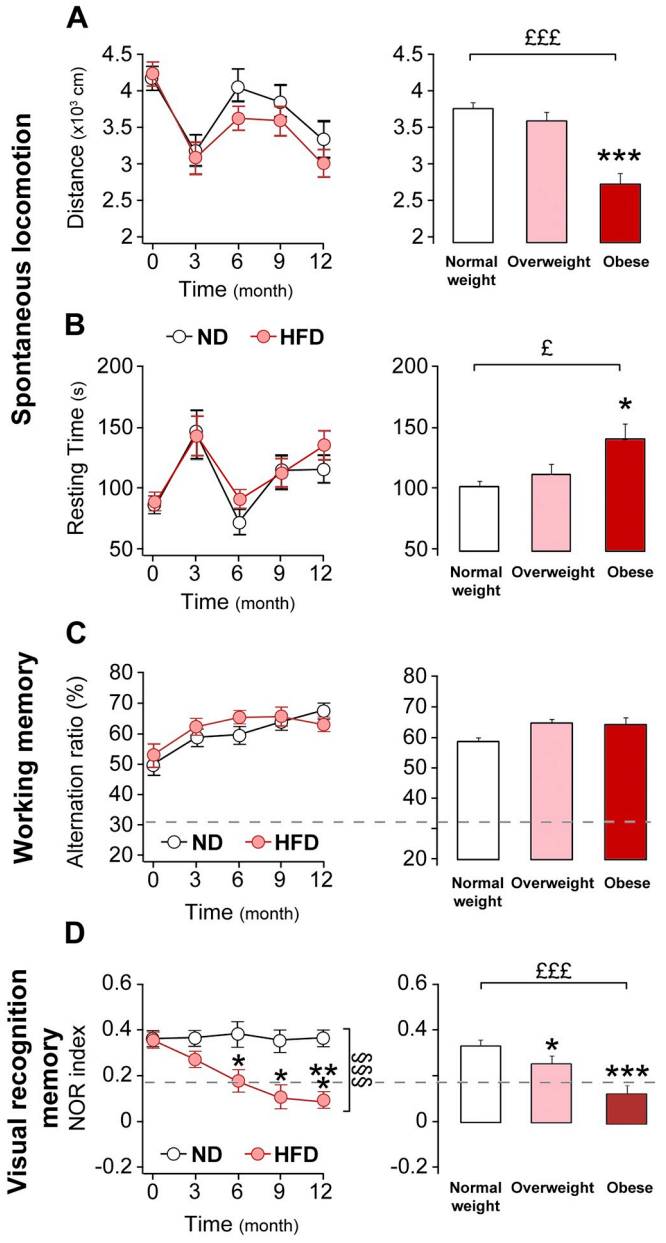

Fig. 3. Spontaneous locomotion, working memory and visual recognition memory of normal diet (ND)- and high fat diet (HFD)-fed mice. Spontaneous locomotion assessed by actimetry test. (A) travelled distance (in 10^3 cm) and (B) resting time (in s). (C) Working memory assessed by spontaneous alternation test. The grey dashed line shows the random alternation. (D) Visual recognition memory assessed by the Novel Object Recognition (NOR) test. The grey dashed line shows the 50% reduction of the memory function. For A, B, C, D, results are depicted according to diet in left panels, and to weight categories in right panels.

Data are shown as mean ± sem. Statistical analysis was performed using a two-way ANOVA, $^{§§§}p < .001$ for the effect of the *Diet* factor; one-way ANOVA $^{£££}p < .01$, $^{£}p < .05$ for the effect of the *Weight categories* factor. Tukey *post hoc* multiple comparisons were performed: *p < .05, ***p < .001 for HFD *vs* ND comparison (2-way ANOVA) or *vs* Normal weight comparison (1-way ANOVA).

memory retention was similar whatever the diet (Fig. 4B, left panels, Ret_{targ} and Ret_{opp}) or the weight category (Fig. 4B, right panels, Ret_{targ} and Ret_{opp}). No differences were observed between ND- and HFD-fed mice at other time-points (data not shown). Furthermore, during the acquisition training period (week 2), the memory flexibility performance was close between ND- and HFD-fed mice (Fig. 4C, left panel), as well as among normal-weight, overweight, and obese mice (Fig. 4C, right panel). On the probe test, the memory flexibility performance was the same between ND- and HFD-fed mice (Fig. 4D, left panels, Ret_{targ} and Ret_{opp}), but different ($F_{2,120} = 3.34$, $p < 0.05$) among weight categories (Fig. 4D, right panels, Ret_{targ} and Ret_{opp}). Indeed, the time spent in the opposite quadrant was longer ($p < 0.05$) for overweight compared to normal-weight mice. The same tendency was observed in obese mice, but did not reach statistical significance.

3.3. High fat diet impairs cerebral vasomotion, blood flow but not baseline tissue perfusion

Blood flow through the middle cerebral artery (MCA) was lower in HFD- than in ND-fed mice, without fall (2-way ANOVA *Diet*: $F_{1,68} = 24.79$, $p < 0.001$), as evidenced by Doppler laser flowmetry. This difference appeared from 6 months to 12 months after post-hoc multiple comparisons (Fig. 5A). No significant reduction in blood flow was found among weight categories (Fig. 5B).

Baseline brain perfusion was explored by MRI on both anterior and posterior areas. Regions of interest were defined in accordance to behavioral deficits: prefrontal cortex (Fig. 5C, D), hippocampus (Fig. 5E, F) and perirhinal/entorhinal cortex (Fig. 5G, H). Neither the type nor the duration of the diet has changed the baseline brain perfusion (Fig. 5C, E, G). By contrast, hippocampus perfusion was significantly higher in overweight and obese mice compared to normal-weight mice (Fig. 5F; categories: $F_{2,115} = 5.10$, $p < 0.01$: Normal weight 114 ± 4 $mL.min^{-1}.100\,g^{-1}$, Overweight 137 ± 9 $mL.min^{-1}.100\,g^{-1}$, $p < 0.05$, Obese 165 ± 10 $mL.min^{-1}.100\,g^{-1}$, $p < 0.05$).

Vascular reactivity was challenged in MCA and in the same brain areas as mentioned above (Fig. 6), using carbachol (cholinergic relaxation) and phenylephrine (adrenergic constriction). Baseline diameters of MCA were comparable whatever the diet (at 9 months: ND 112.7 ± 3.4 µm *vs* HFD 114.6 ± 5.2 µm). Carbachol-induced endothelium-dependent relaxation has decreased significantly in HFD-fed mice at 9 months in the MCA (*Diet* $F_{1,42} = 17.48$, $p < 0.001$: ND 25.5 ± 10.8% *vs* HFD 10.7 ± 4.8%, $p < 0.05$ Fig. 6A), whereas no significant modification of the phenylephrine-induced contractile response was observed (Fig. 6B). In the prefrontal cortex, carbachol-induced endothelium-dependent relaxation has decreased significantly in HFD-fed mice at 9 months (*Diet* $F_{1,48} = 10.75$, $p < 0.01$: ND 20.1 ± 3.7% *vs* HFD -0.8 ± 4.6%, $p < 0.05$), at 12 months (ND 21.3 ± 4.2% *vs* HFD 3.4 ± 1.1%, $p < 0.01$, Fig. 6C), and tended to decrease clearly in obese mice ($p = 0.065$, Fig. 6D). The contractile response to phenylephrine did not change significantly in overweight or obese mice, whereas the contractile response to endothelin-1 was significantly reduced in obese mice ($p = 0.032$). The sodium nitroprusside (SNP)-induced smooth muscle-dependent relaxation tended to decrease in overweight and obese mice ($p = 0.146$, Fig. 6D). In the hippocampus, carbachol-induced endothelium-dependent relaxation has decreased significantly in HFD-fed mice at 9 months (*Diet* $F_{1,49} = 6.93$, $p < 0.05$: ND 32.3 ± 7.6% *vs* HFD -0.6 ± 3.9%, $p < 0.01$) and at 12 months (ND 28.4 ± 6.9% *vs* HFD 6.1 ± 3.9%, $p < 0.05$, Fig. 6E). This endothelium-dependent relaxation tended to decrease clearly in obese mice ($p = 0.051$), while the contractile response to phenylephrine or endothelin-1, as well as the smooth muscle-dependent relaxation induced by SNP did not change (Fig. 6F). All values are summarized in Table 3.

Whatever the group and time point, no magnetic field perturbation was found in MRI, accounting for tissue injury (T2/ADC), microbleed (SWI), or subtle local water change (FLAIR, Appendix Fig. A.2). The preservation of capillary blood-brain barrier permeability or patency was confirmed by histology using the FITC dextran tracer, which did

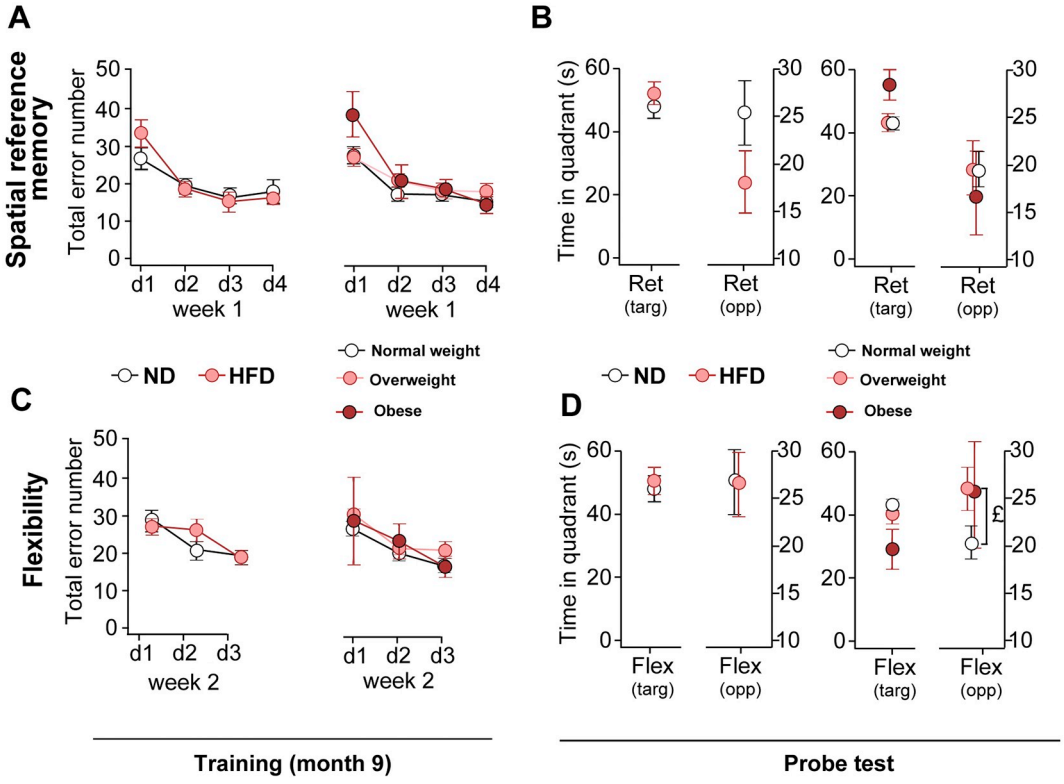

Fig. 4. Spatial reference memory and memory flexibility assessment with the Barnes Maze after 9 months of ND or HFD diet. Spatial reference memory: acquisition training for the 1st week represented by the number of total errors (A), and time spent in target or opposite quadrants on the test day at the end of the 1st week (Retrieval task, Ret, B). Memory flexibility: acquisition training for the 2nd week represented by the number of total errors (C), and time spent in target or opposite quadrants on the test day at the end of the 2nd week (Flexibility task, Flex, D). For A, B, C, D, results are depicted according to diet in left panels, and to weight categories in right panels.
Data are shown as mean ± sem. Statistical analysis was performed using a two-way ANOVA for the effect of the *Diet* factor; one-way ANOVA $^{£}p < .05$ for the effect of the *Weight categories* factor.

not show any blurred or dropped signal respectively (Appendix Fig. A.3). As well, neither microinfarct nor microhemorrhage was found after histological examination (hematoxylin/eosin, Appendix, Fig. A.4).

3.4. Visceral adiposity correlates with a reduced endothelial relaxation and both impaired visual recognition memory and flexibility

Several statistical correlations were tested in order to authenticate associations between metabolic disturbances, cognitive deficit and vascular dysfunction (Fig. 7A), and are summarized in Table 4. Significant correlations were found between visceral adipose tissue deposition and NOR index (Kendall's rank coefficient -0.27, $p < 0.001$, power = 0.96), flexibility (Kendall's rank coefficient 0.15, $p < 0.05$, power = 0.38), or carbachol response (Pearson's correlation coefficient -0.46, $p < 0.001$, power = 0.99). Statistical fit models were applied on the same datasets for extrapolation purposes, and were expressed as a percentage of maximal averaged response (bold curves, Fig. 7B), in order to predict the loss of cognitive (black curve) and vascular functions (endothelium-dependant dilation, red curve) according to visceral adipose tissue deposition. Curves of functional loss were superimposed. Indeed, a 50% loss of cognitive function was observed for 2.42 g of visceral fat. Similarly, a 50% loss of vascular function was observed for 2.69 g of visceral fat.

4. Discussion

Here we describe a follow-up cohort of mice until midlife, after up to one year of free access HFD or ND, without physical exercise. This approach simulated a "naturally-occurring" weight gain and dyslipidemia, accounting for the lifestyle of a modern young population until the middle age. We demonstrate for the first time the influence of diet-induced visceral adiposity as a midlife risk factor for premature cognitive dysfunction.

Experimental works on this topic have been mostly carried out using genetically engineered rodent models in which early and severe metabolic responses to diet were uniformly observed (Wong et al., 2016), or using high-sugar diet (fructose or sucrose), very high-fat diet (60% fat), or a combination of both (Buettner et al., 2007; Panchal and Brown, 2011). A 40% animal-derived fat-enriched diet ("high fat") was preferred here to induce progressive metabolic disturbances. The HFD imposed to our mice resulted in an accelerated weight gain, a high visceral fat deposition and a decrease in the ability to clear blood glucose from 3 months of diet. Likewise, a modified blood lipid profile and hepatic fat accumulation were observed from 6 months of diet. These metabolic disorders are classically associated with HFD (Buettner et al., 2007). But surprisingly, the normal diet was able to induce overweight (> 36 g) in 20% of our mice population after 6 months, confirming the impact of the sedentary nature of standard housing conditions and the propensity of C57Bl/6 mice to develop a late onset obesity (Becskei et al., 2010; Lautenschlager et al., 2008). This finding is all the more noteworthy since our mice had *ad libitum* access to food and water over a long period (52 weeks), possibly introducing variations in food intake.

Obese animals obtained after a short-term enriched diet are prominently examined in preclinical studies (Wong et al., 2016), reducing the opportunity of observing heterogeneous responses to diet. The heterogeneity observed here has opened possible avenue to correlate

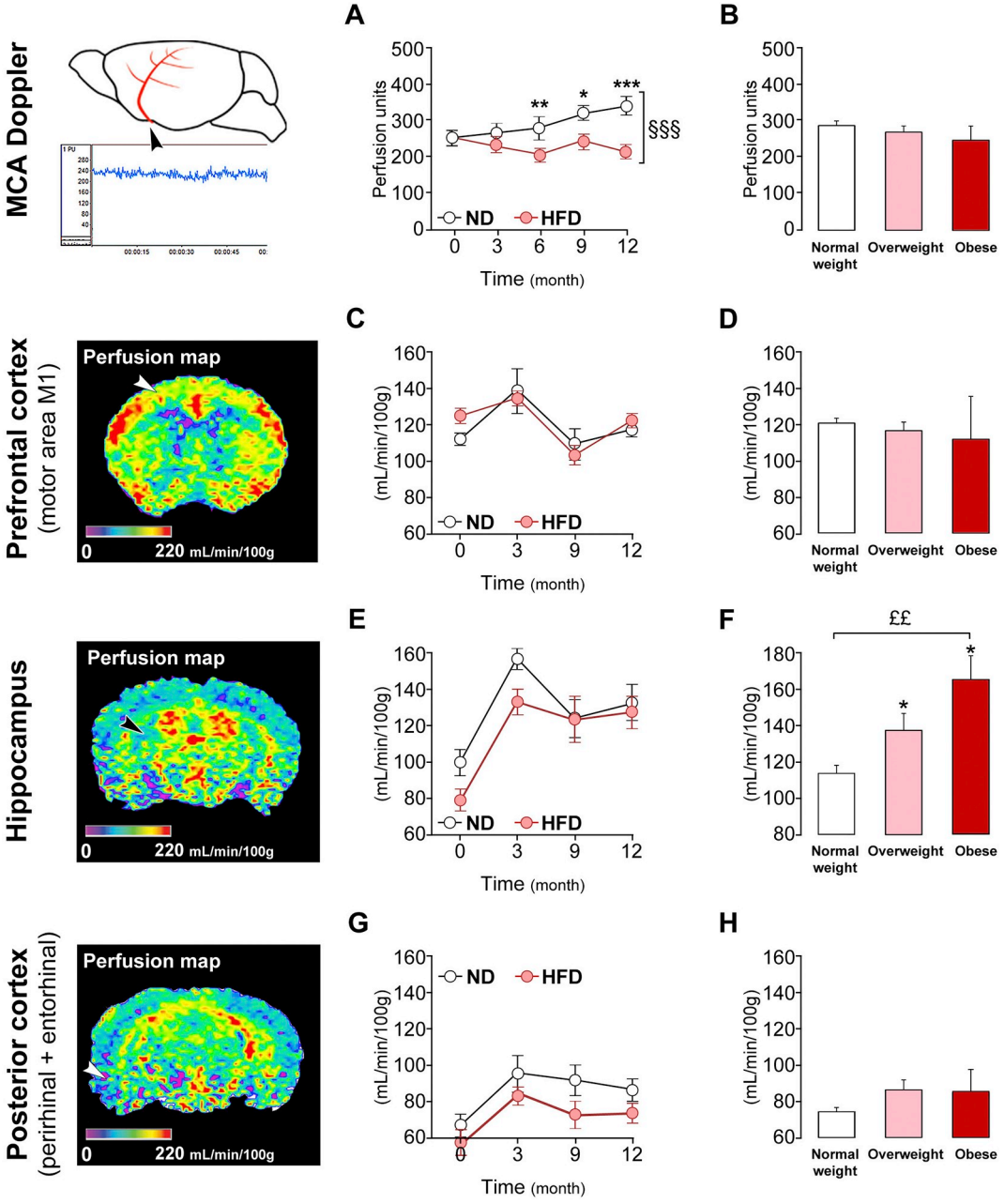

Fig. 5. Changes in cerebral blood flow and brain tissue perfusion in ND- and HFD-fed mice. (A, B) Cerebral blood flow was recorded by laser Doppler in the middle cerebral artery (MCA) area *in vivo* on anesthetized ND- and HFD-fed mice. (C to H) Quantification of the brain tissue perfusion assessed by MRI. Representative perfusion maps (left panel) and respective values of tissue perfusion recorded in prefrontal cortex (C, D) for the anterior area or in hippocampus (E, F) and perirhinal/entorhinal cortex (G, H) for the posterior areas.

Data are shown as mean ± sem. Statistical analysis was performed using a two-way ANOVA, $^{§§§}p < .001$ for the effect of the *Diet* factor; or one-way ANOVA, $^{ff}p < .01$ for weight categories. Tukey *post hoc* analysis was performed: $^{*}p < .05$, $^{**}p < .01$ and $^{***}p < .001$ for HFD *vs* ND comparison (2-way ANOVA) or *vs* Normal weight (1-way ANOVA).

weight gain with metabolic parameters. For instance, our obese mice exhibited impaired glucose tolerance, but also a moderate fasting hyperglycemia of 1.3 g/L, far from the diabetic rodent models induced by streptozotocin, which exhibit a fasting glycemia above 3 g/L in one week (Ramos-Rodriguez et al., 2015). One cannot rule out possible progression of this middle-aged glycemic disturbance towards a diabetic disease. The setting of an overweight category of mice coming from both ND and HFD groups enabled us to select visceral adipose tissue (VAT) (Table 3) as the metabolic parameter that was the best correlated with weight gain, in order to better define associations between metabolic disturbance, and both cognitive and vascular functions.

The long-term HFD did not reduce the learning abilities, spatial reference memory or working memory. Other studies have

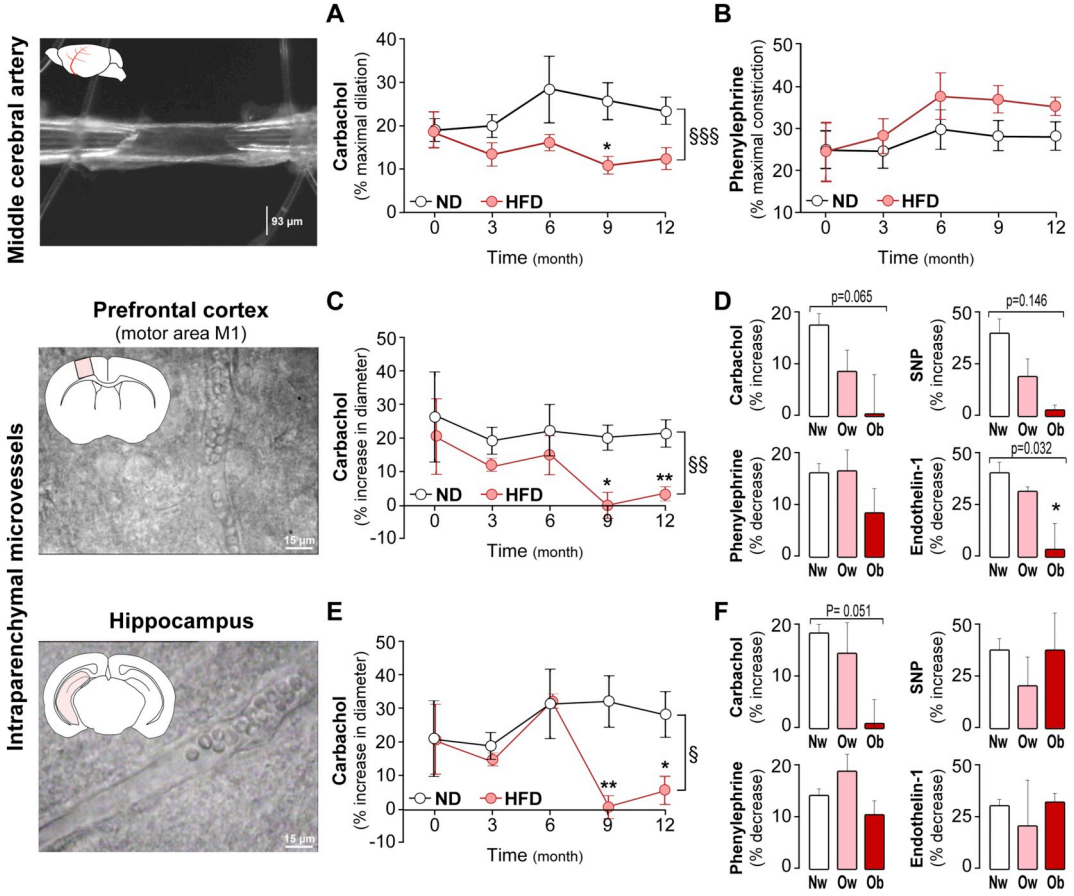

Fig. 6. Changes in vascular reactivity of cerebral macro- and microvessels for ND- and HFD-fed mice. For each row, the left column depicts the preparation as the middle cerebral artery or microvessels in brain slices. (A, B) Reactivity of the middle cerebral artery was assessed with a Halpern arteriograph in response to 0.1 µM carbachol (% increase diameter) (A) or 30 µM phenylephrine (% constriction) (B). Microvascular reactivity was similarly assessed in prefrontal cortex for the anterior area (C) and in hippocampus for the posterior area (E). The profile of vasoactive functions has assessed for each weight categories (Nw: normal weight; Ow: overweight; Ob: obese) using various vasoactive compounds (SNP: sodium nitroprusside; D, F).
Data are shown as mean ± sem. Statistical analysis was performed using a two-way ANOVA, $^{§§§}p < .01$, $^{§§}p < .01$, $^{§}p < .05$ for the effect of the *Diet* factor or one-way ANOVA for weight categories. Tukey *post hoc* analysis was performed: $^{*}p < .05$, $^{**}p < .01$ for HFD *vs* ND comparison (2-way ANOVA) or *vs* Normal weight (1-way ANOVA).

demonstrated an altered working memory but after a HFD of > 12 months (Toyama et al., 2015) or when the diet was started in younger animals such as 5 week-old (Wang et al., 2018) compared to 8 week-old mice in the present study. The early life period between weaning and adulthood appears particularly vulnerable to the deleterious effect of HFD consumption and could explain the discrepancy (Boitard et al., 2012). Furthermore, HFD-fed mice showed an impaired visual recognition memory from 6 months. Such an early impairment has not been reported yet, suggesting that this type of cognitive function should be tested more frequently in such experimental studies. This impaired

Table 3
Vascular reactivity of cerebral microvessels maximal responses (%) assayed for mice weight categories.

	Relaxation (%)				Constriction (%)			
	Carb		SNP		Phe		ET-1	
	PFC	Hipp	PFC	Hipp	PFC	Hipp	PFC	Hipp
Normal weight	17.3 ± 2.4	17.9 ± 2.2	39 ± 7.4	37.9 ± 4.9	16 ± 1.8	21 ± 1.6	40.4 ± 4.7	30 ± 3.1
Overweight	8.5 ± 4.3	14.2 ± 6	19.5 ± 8	20 ± 14.3	16 ± 4.3	28 ± 5.2	31 ± 1.6	20 ± 21.9
Obese	−0.3 ± 7.6	−0.8 ± 5.6	3 ± 0.6	37 ± 18.2	8 ± 2.8	15 ± 4.1	3 ± 12.6	31 ± 4.4
Normal weight	=	=	=	=	=	=	=	=
Overweight	↘	=	=	=	=	=	=	=
Obese	↘↘	↘↘	↘↘	=	↘	=	↘	=

(Carb: carbachol; SNP: sodium nitroprusside; Phe: phenylephrine; ET-1: endothelin 1; PFC: prefrontal cortex; Hipp: hippocampus). Results are expressed in mean ± SEM.

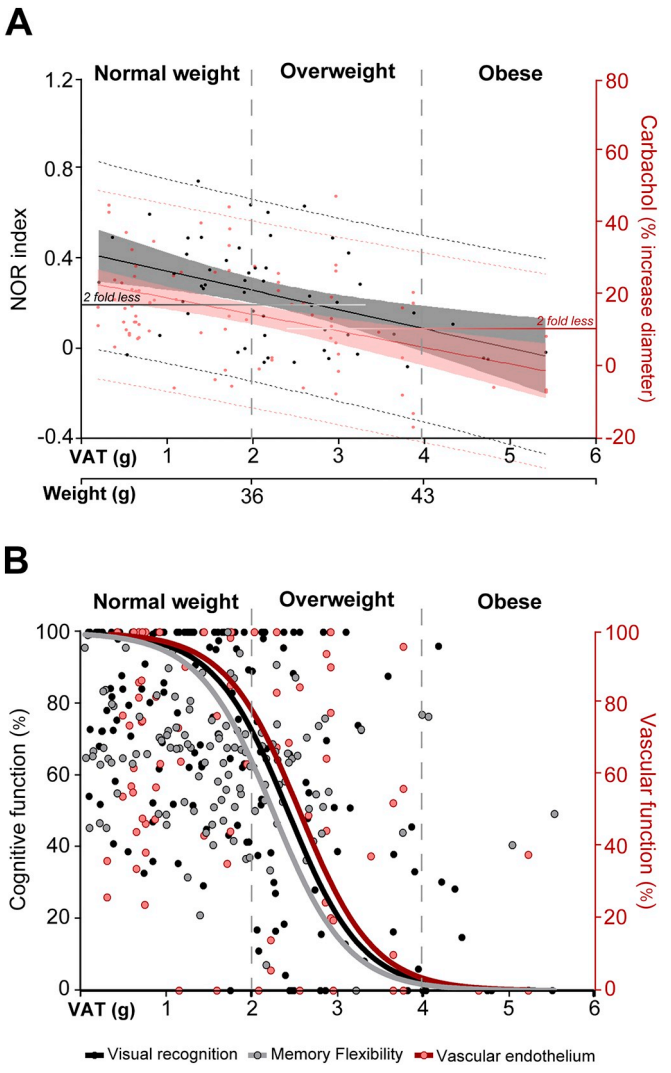

Fig. 7. Association plot between metabolic, cognitive and vascular parameters. (A) Experimental associations between visceral adipose tissue deposition (VAT in g) and Novel object recognition (NOR) index (black circles, black line), or vascular endothelium-dependent response to carbachol (red circles, red line). (B) Statistical extrapolation from experimental data expressed as a percentage of maximal averaged response for NOR index (black circles), memory flexibility (grey circles) and carbachol response (pink circles). Bold curves represented the statistical models of the loss of cognitive (black and grey curves) and vascular (red curve) function associated with VAT deposition. (For interpretation of the references to colour in this figure legend, the reader is referred to the web version of this article.)

ability to discriminate a novel object was worsened at 12 months, but was one of the two cognitive functions found altered out of the four tested in our experimental conditions. This has been observed in studies including a later introduction of HFD (in mice between 7 to 24 months of age), with a higher percent of fat (60%), and for a shorter duration (2–5 months) (Carey et al., 2014; Kesby et al., 2015; Valcarcel-Ares et al., 2019). Since a protective effect of weight gain and high lipidemia in older adults has been put forward (Atti et al., 2008; Mielke et al., 2005), investigating the deleterious effect of high fat diet in very old mice might be of limited relevance, in the perspective of an efficient

Table 4
Statistical correlations between metabolic disturbances, cognitive deficit and vascular dysfunction.

	Observation (n)	Coefficient (r)	Power (> 0.80)	Significance (p=)
Correlation *vs* weight				
Triglycerides	233	0.014	0.05	0.754
Total cholesterol	233	0.269	0.99	$2.2\ 10^{-16}$
HDL cholesterol	232	0.281	0.99	$2.2\ 10^{-16}$
NonHDL cholesterol	232	0.106	0.36	0.017
Fasting glycemia	184	0.325	0.99	$2.2\ 10^{-16}$
OGTT (AUC)	183	0.282	0.97	$2.2\ 10^{-16}$
NOR index	173	−0.244	0.90	$1.9\ 10^{-6}$
Flexibility	122	0.143	0.35	0.020
Carbachol (%)	84	−0.383	0.96	$3.2\ 10^{-4}$
Correlation *vs* VAT				
Triglycerides	88	0.020	0.05	0.781
Total cholesterol	88	0.292	0.80	$5.7\ 10^{-5}$
HDL cholesterol	88	0.363	0.94	$5.9\ 10^{-7}$
NonHDL cholesterol	88	0.130	0.23	0.073
Fasting glycemia	57	0.195	0.30	0.034
OGTT (AUC)	57	0.296	0.62	0.001
NOR index	173	−0.273	0.96	$9.9\ 10^{-8}$
Flexibility	122	0.148	0.38	0.016
Carbachol (%)	84	−0.466	0.99	$8.1\ 10^{-6}$

(NOR: novel object recognition; OGTT: oral glucose tolerance test).

intervention on the diet-induced risk factor or deleterious mechanism. Rather than diet, weight was the most prominent risk factor for the impairment of the prefrontal cortex-based memory flexibility, since observed in our overweight and obese mice. Indeed, these mice had a lesser ability to integrate the new location of the escape box, and the obese mice had a reduced spontaneous motricity, probably as a consequence of extreme weight rather than a neurological deficit.

Overall, our mice exhibit a mild impairment of visual recognition memory and memory flexibility, both associated to weight gain and visceral adiposity at middle-age, consistently with previous human studies (Hassing et al., 2010). The brain areas involved in these functions are respectively the perirhinal posterior cortex and the prefrontal cortex (Barker and Warburton, 2011; Latif-Hernandez et al., 2016; Winters et al., 2008), which are required for complex executive functions. Accordingly, our mice may present a disturbance of the "updating" factor as described by Miyake et al. (2000) for better understanding the ability of humans to integrate new elements for the execution of complex tasks (Miyake et al., 2000). Our study demonstrated that a high but progressive weight gain in middle-aged mice, free from installed cardiovascular or neurodegenerative disease, gave rise to a lower performance on tests that challenge cognitive functions considered as of higher order, as executive functions in humans. Executive functions are theorized to affect activities of daily living (Baddeley, 1998; Logue and Gould, 2014; Stuss and Alexander, 2000). The impaired visual recognition memory, which was observed in overweight mice, is reported in patients in early course of mild cognitive impairment (MCI) (Barbeau et al., 2004; Valenti et al., 2017; Wolk et al., 2008). In humans, such an impairment could be barely symptomatic, hindering the trigger of a cognitive complaint. Efforts are made towards identifying and ranking MCI patients at risk of Alzheimer's disease (Zhou et al., 2012). In 2007, Gunstad et al. have reported a link between high body mass index and low performance on cognitive tests, especially a reduced executive function (Gunstad et al., 2007). The etiology of this disorder remains unclear, but increasing evidences

suggest that cerebrovascular alteration contribute to the development of cognitive impairment (Duncombe et al., 2017; Toth et al., 2016).

Cerebrovascular dysfunctions were found in small parenchymal arteries of the brain areas defined in accordance to behavioral paradigms. The impairment pattern of vasomotion was different among brain areas. The endothelium-dependent relaxation was lower in both hippocampus and prefrontal cortex. Moreover, only in the latter area, the endothelium-independent relaxation and the contractile responses were more severely impaired in obese than in other mice weight categories (Table 3). Structural hypotheses for such dysfunctions have been drawn from several studies reporting microvascular tortuosity (Chesnutt and Han, 2011, 2013), increase in artery wall thickness (Tümer et al., 2014), or other parietal changes in the pial arteries (Kang et al., 2016), all possibly increasing the resistance to blood flow. Likewise, the MCA of HFD-fed mice showed a shortened carbachol-sensitive relaxation, associated to a reduced blood flow in the Sylvian territory, underlining the loss of the MCA adaptability to changes in vascular resistance. These dysfunctions of both MCA and cerebral arterioles could reduce the brain tissue perfusion, which was however not found in our study, neither by MRI nor after fluorescent tracer analysis of the microvascular patency and blood-brain barrier permeability. These results rather suggest a less efficient neurovascular coupling upon stimulation, which might reduce cognitive performance at middle age.

The statistical extrapolation of our results shows a synchronous decline in cognitive and vascular impairments, along the increase of visceral adipose tissue deposition, suggesting a direct link between vascular impairment and cognitive decline processes. Therefore, we believe that measuring both visceral adipose tissue and vascular function at middle age would help identify subjects at risk of underlying decline of cognitive functions. Determining vascular function is easily performed in the periphery, through a digital plethysmograph device. Whether such a measurement can reflect cerebral vascular dysfunction remains however unknown and needs further investigation. For middle-aged subjects at risk, executive functions could then be tested, and impairment would urge the need for memory care, and for a lowering of metabolic risk factors through nutritional education rather than pharmacological treatment.

5. Conclusion

Young adult mice exposed to high-fat diet are prone to develop a mild impairment of some specific cognitive functions at middle-age. Whether this might contribute to a precipitated dependency in the late life, needs to be proven. Weight gain, metabolic disturbances and associated cerebrovascular dysfunction are statistical parameters able to predict cognitive decline and should be considered as potential tools for early diagnosis.

Acknowledgments

We warmly thank Prof Anne Muhr-Tailleux for her great technical assistance in blood assays (U1011-European Genomic Institute, Lille). We also thank F. Auger and N. Durieux (from the University of Lille's *in vivo* imaging core facility), C. Laloux (from the SFR DN2M functional testing core facility), M. Tardivel (from the Lille Bioimaging Centre) for her great technical assistance in fluorescent Dextran microscopy technical advice and access to equipment and the Lille Animal Facility.

This work was supported by the French Ministry for Research and Higher Education and the Conseil Régional des Hauts de France, as well as the VasCog Research Network, Lille, France.

Declaration of Competing Interest

The authors have declared that no conflict of interest exists.

Appendix A

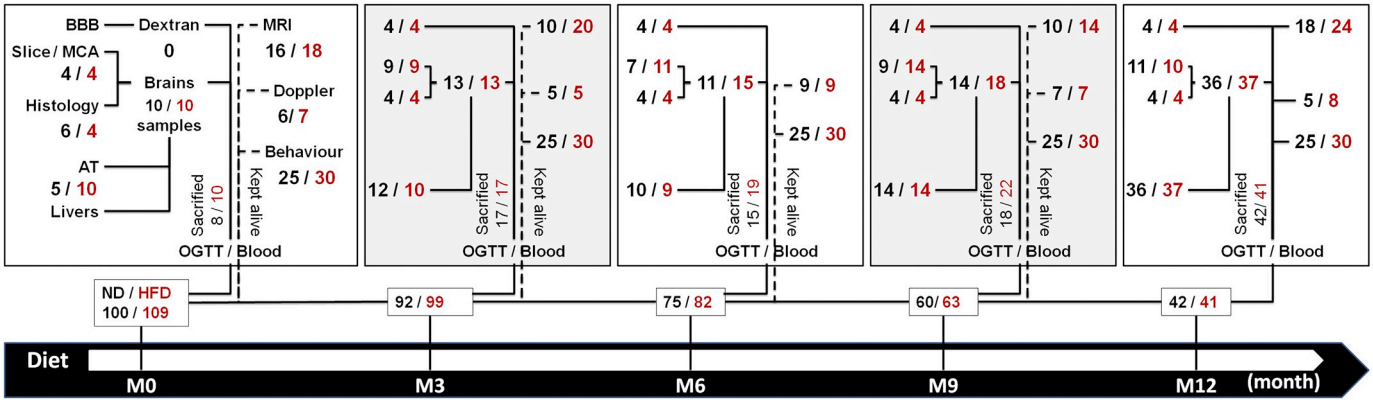

Fig. A.1. An overview of the design for the experiment. After one week of acclimation the animals were randomly distributed into two experimental groups: a normal diet-fed mice group (ND, n = 100 in black) and a high fat diet-fed group (HFD, n = 109 in red). At the start of the protocol (M0), blood sampling and oral glucose tolerance test (OGTT) were realized, behavior state was assessed, MRI study was conducted and a part of the animals was sacrificed for tissue sampling. These tests were repeated at 3 (M3), 6 (M6), 9 (M9) and 12 (M12) months. (For interpretation of the references to colour in this figure legend, the reader is referred to the web version of this article.)

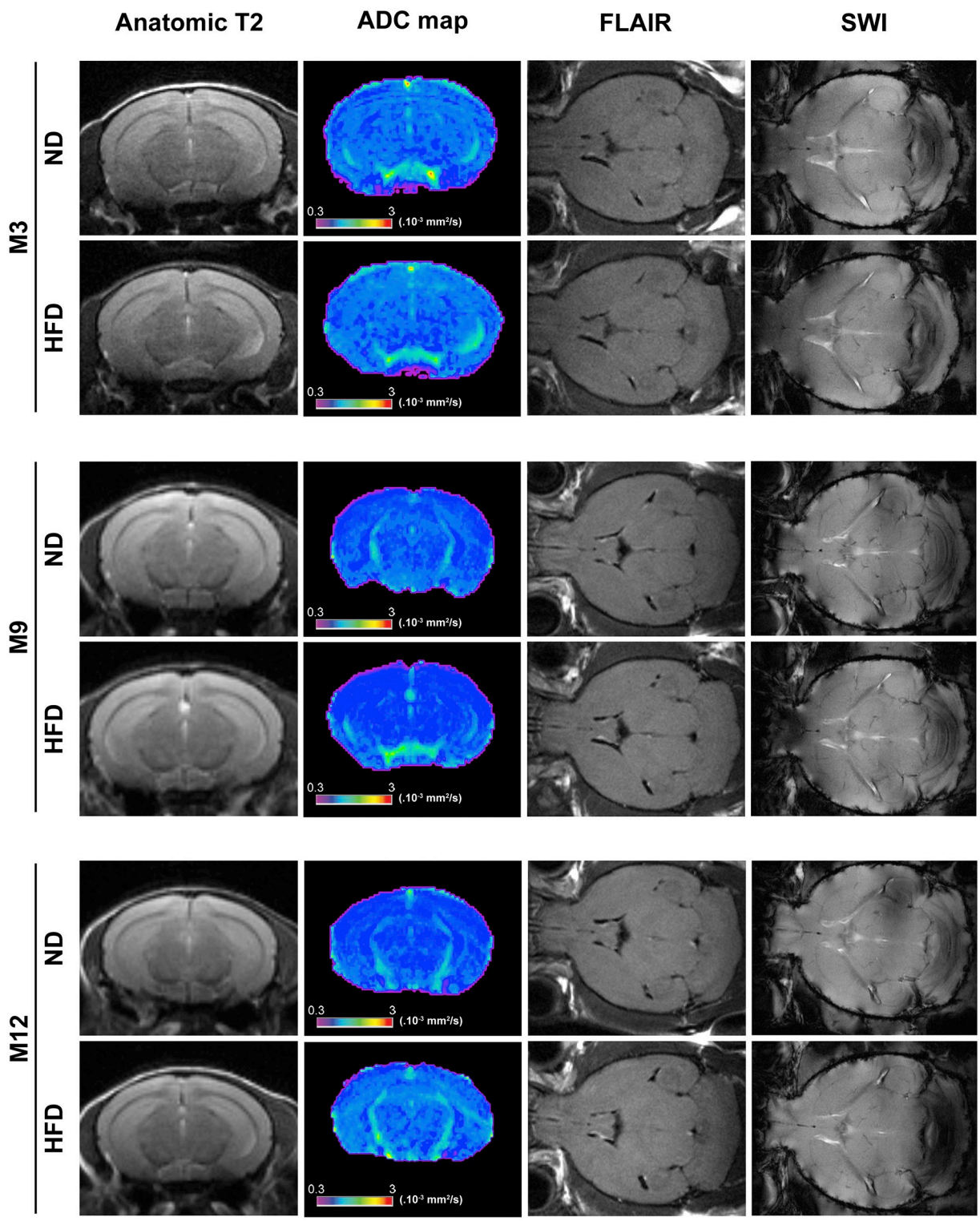

Fig. A.2. Absence of change in magnetic properties of the brain of normal diet (ND)- and high fat diet (HFD)-fed mice. Images are representative of brain from mice after 3, 9 or 12 months of ND or HFD. Neither abnormal organization of brain structures (T2-anatomical slices) nor disturbances of tissue water content (ADC maps) were observed. No microbleed (SWI: susceptibility-weighted imaging) or other sign of local water anomaly and/or vascular defect (FLAIR: fluid-attenuated inversion and recovery imaging) was noticed either.

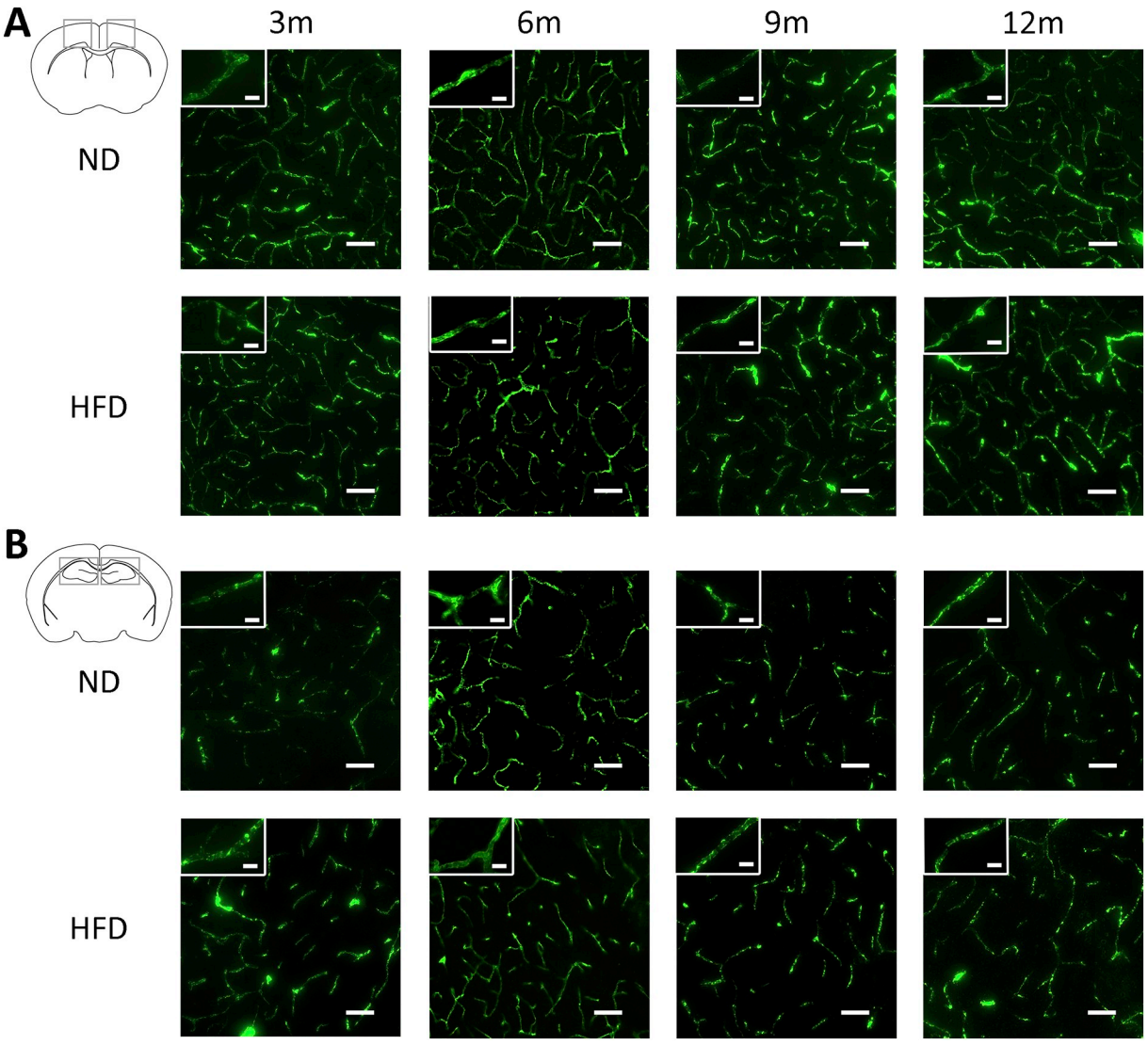

Fig. A.3. Absence of change in microvascular patency and blood-brain barrier integrity in the brains of normal diet (ND)- and high fat diet (HFD)-fed mice. Images are representative fields of view (square windows) of the prefrontal cortex (A) and hippocampus (B) brain areas from mice after 3, 6, 9 or 12 months (m) of ND or HFD. Brain slices from fluorescein isothiocyanate (FITC)-Dextran-infused animals illustrate the microvascular patency as well as the BBB integrity (Scale bar = 50 μm). No change in the microvascular patency was observed throughout the brain slices since the fluorescence signal was uniformly ramified in each brain area. The blood-brain barrier integrity was preserved as no blurred fluorescence signal was found alongside the capillary segments. Magnified images (inner windows) illustrate typical morphology of capillaries in each field of view, as revealed by exclusively intravascular FITC-Dextran signals as a marker of a tight blood-brain barrier (scale bar = 10 μm). n = 3 to 6 animals per group, from 3 independent experiments.

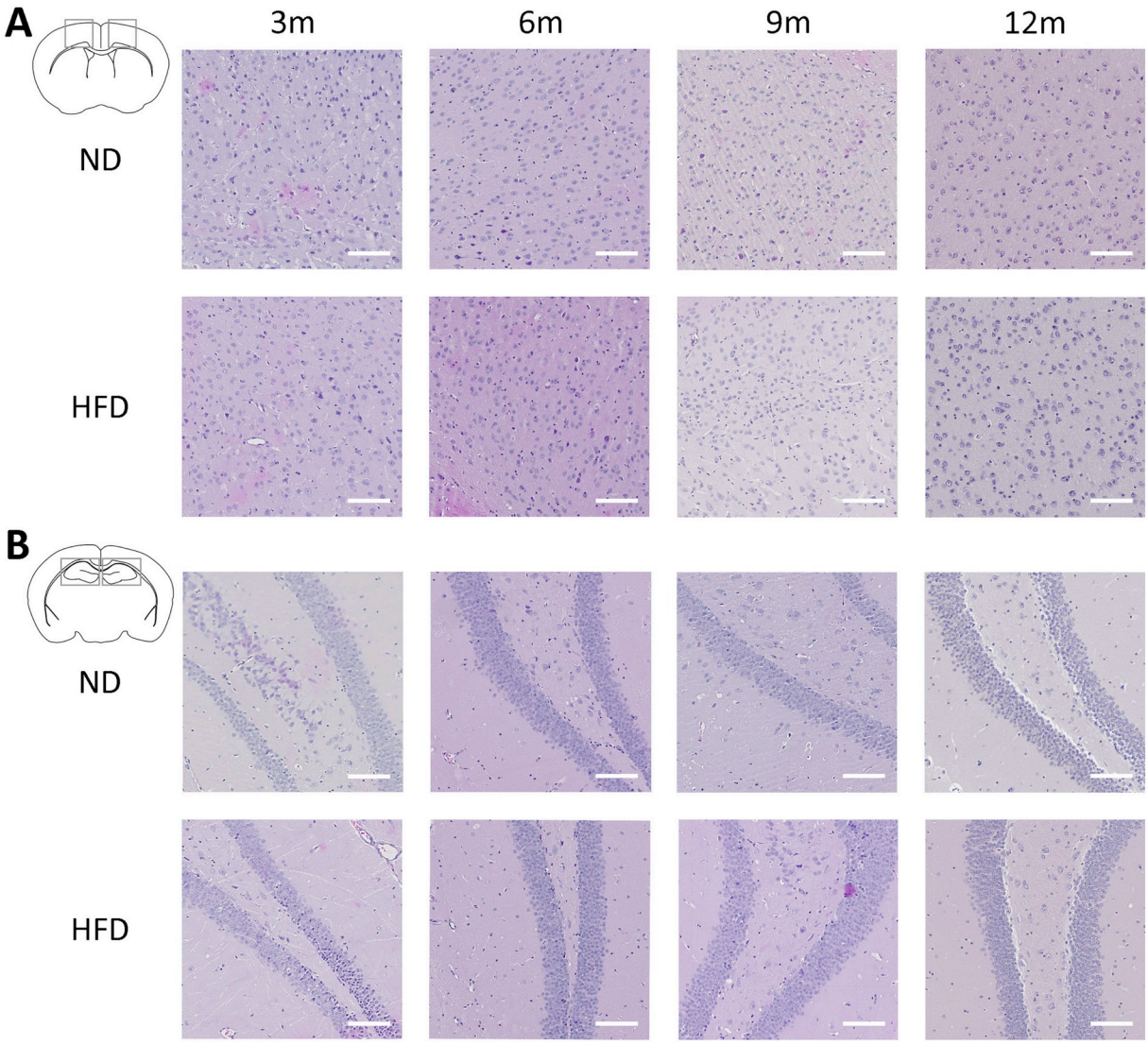

Fig. A.4. Absence of neuropathological lesion in the brains of normal diet (ND)- and high fat diet (HFD)-fed mice. Images are representative fields of view (square windows) of the prefrontal cortex (A) and hippocampus (B) brain areas from mice after 3, 6, 9 or 12 months (m) of ND or HFD. Coronal sections were stained with hematoxylin/eosin and observed under a bright-field microscope. Neuropathological examination revealed neither tissue loss nor abnormal organization. No microbleed or other sign of vascular alteration was noticed either. Scale bar = 50 µm; n = 3 to 6 animals per group, from 3 independent experiments.

References

Antunes, M., Biala, G., 2012. The novel object recognition memory: neurobiology, test procedure, and its modifications. Cogn. Process. 13, 93–110.

Atti, A.R., Palmer, K., Volpato, S., Winblad, B., Ronchi, D.D., Fratiglioni, L., 2008. Late-life body mass index and dementia incidence: nine-year follow-up data from the Kungsholmen project. J. Am. Geriatr. Soc. 56, 111–116.

Baddeley, A., 1998. Working memory. C. R. Acad. Sci. III Sci. Vie 321, 167–173.

Barbeau, E., Didic, M., Tramoni, E., Felician, O., Joubert, S., Sontheimer, A., Ceccaldi, M., Poncet, M., 2004. Evaluation of visual recognition memory in MCI patients. Neurology 62, 1317–1322.

Barker, G.R.I., Warburton, E.C., 2011. When is the hippocampus involved in recognition memory? J. Neurosci. 31, 10721–10731.

Becskei, C., Lutz, T.A., Riediger, T., 2010. Reduced fasting-induced activation of hypothalamic arcuate neurons is associated with hyperleptinemia and increased leptin sensitivity in obese mice. Am. J. Phys. Regul. Integr. Comp. Phys. 299, R632–R641.

Boitard, C., Etchamendy, N., Sauvant, J., Aubert, A., Tronel, S., Marighetto, A., Layé, S., Ferreira, G., 2012. Juvenile, but not adult exposure to high-fat diet impairs relational memory and hippocampal neurogenesis in mice. Hippocampus 22, 2095–2100.

Buettner, R., Schölmerich, J., Bollheimer, L.C., 2007. High-fat diets: modeling the metabolic disorders of human obesity in rodents. Obesity (Silver Spring) 15, 798–808.

Carey, A.N., Gomes, S.M., Shukitt-Hale, B., 2014. Blueberry supplementation improves memory in middle-aged mice fed a high-fat diet. J. Agric. Food Chem. 62, 3972–3978.

Stephane, Champely, 2018. Basic Functions for Power Analysis. R package version 1.2-2, (November 21th, 2018). https://CRAN.R-project.org/package=pwr.

Chesnutt, J.K.W., Han, H.-C., 2011. Tortuosity triggers platelet activation and thrombus formation in microvessels. J. Biomech. Eng. 133, 121004.

Chesnutt, J.K.W., Han, H.-C., 2013. Platelet size and density affect shear-induced thrombus formation in tortuous arterioles. Phys. Biol. 10, 056003.

Costa, R.M., Neves, K.B., Tostes, R.C., Lobato, N.S., 2018. Perivascular adipose tissue as a relevant fat depot for cardiovascular risk in obesity. Front. Physiol. 9.

Debette, S., 2013. Vascular risk factors and cognitive disorders. Rev. Neurol. (Paris) 169, 757–764.

Duncombe, J., Kitamura, A., Hase, Y., Ihara, M., Kalaria, R.N., Horsburgh, K., 2017. Chronic cerebral hypoperfusion: a key mechanism leading to vascular cognitive impairment and dementia. Closing the translational gap between rodent models and human vascular cognitive impairment and dementia. Clin. Sci. 131, 2451–2468.

Francis, H., Stevenson, R., 2013. The longer-term impacts of Western diet on human cognition and the brain. Appetite 63, 119–128.

González, H.M., Tarraf, W., Harrison, K., Windham, B.G., Tingle, J., Alonso, A., Griswold, M., Heiss, G., Knopman, D., Mosley, T.H., 2018. Midlife cardiovascular health and 20-year cognitive decline: atherosclerosis risk in communities study results. Alzheimers Dement. 14, 579–589.

Gunstad, J., Paul, R.H., Cohen, R.A., Tate, D.F., Spitznagel, M.B., Gordon, E., 2007. Elevated body mass index is associated with executive dysfunction in otherwise healthy adults. Compr. Psychiatry 48, 57–61.

Haley, M.J., Mullard, G., Hollywood, K.A., Cooper, G.J., Dunn, W.B., Lawrence, C.B., 2017. Adipose tissue and metabolic and inflammatory responses to stroke are altered

in obese mice. Dis. Model. Mech. 10, 1229–1243.
Hassing, L.B., Dahl, A.K., Pedersen, N.L., Johansson, B., 2010. Overweight in midlife is related to lower cognitive function 30 years later: a prospective study with longitudinal assessments. Dement. Geriatr. Cogn. Disord. 29, 543–552.
Hidaka, N., Suemaru, K., Li, B., Araki, H., 2008. Effects of repeated electroconvulsive seizures on spontaneous alternation behavior and Locomotor activity in rats. Biol. Pharm. Bull. 31, 1928–1932.
Kang, H.-M., Sohn, I., Jung, J., Jeong, J.-W., Park, C., 2016. Age-related changes in pial arterial structure and blood flow in mice. Neurobiol. Aging 37, 161–170.
Kesby, J.P., Kim, J.J., Scadeng, M., Woods, G., Kado, D.M., Olefsky, J.M., Jeste, D.V., Achim, C.L., Semenova, S., 2015. Spatial cognition in adult and aged mice exposed to high-fat diet. PLoS ONE 10, e0140034.
Kivipelto, M., Ngandu, T., Laatikainen, T., Winblad, B., Soininen, H., Tuomilehto, J., 2006. Risk score for the prediction of dementia risk in 20 years among middle aged people: a longitudinal, population-based study. Lancet Neurol. 5, 735–741.
Latif-Hernandez, A., Shah, D., Ahmed, T., Lo, A.C., Callaerts-Vegh, Z., Van der Linden, A., Balschun, D., D'Hooge, R., 2016. Quinolinic acid injection in mouse medial prefrontal cortex affects reversal learning abilities, cortical connectivity and hippocampal synaptic plasticity. Sci. Rep. 6.
Lautenschlager, N.T., Cox, K.L., Flicker, L., Foster, J.K., van Bockxmeer, F.M., Xiao, J., Greenop, K.R., Almeida, O.P., 2008. Effect of physical activity on cognitive function in older adults at risk for Alzheimer disease: a randomized trial. JAMA 300, 1027–1037.
Lawrence, M.A., 2016. Easy Analysis and Visualization of Factorial Experiments. R package version 4.4-0, (November 21th, 2018). https://CRAN.R-project.org/package=ez.
Livingston, G., Sommerlad, A., Orgeta, V., Costafreda, S.G., Huntley, J., Ames, D., Ballard, C., Banerjee, S., Burns, A., Cohen-Mansfield, J., Cooper, C., Fox, N., Gitlin, L.N., Howard, R., Kales, H.C., Larson, E.B., Ritchie, K., Rockwood, K., Sampson, E.L., Samus, Q., Schneider, L.S., Selbæk, G., Teri, L., Mukadam, N., 2017. Dementia prevention, intervention, and care. Lancet 390, 2673–2734.
Logue, S.F., Gould, T.J., 2014. The neural and genetic basis of executive function: attention, cognitive flexibility, and response inhibition. Pharmacol. Biochem. Behav. 123, 45–54.
Lourenco, J., Serrano, A., Santos-Silva, A., Gomes, M., Afonso, C., Freitas, P., Paul, C., Costa, E., 2018. Cardiovascular risk factors are correlated with low cognitive function among older adults across Europe based on the SHARE database. Aging Dis. 9, 90–101.
Marche, K., Danel, T., Bordet, R., 2011. Fetal alcohol-induced hyperactivity is reversed by treatment with the PPARα agonist fenofibrate in a rat model. Psychopharmacology 214, 285–296.
Mielke, M.M., Zandi, P.P., Sjögren, M., Gustafson, D., Ostling, S., Steen, B., Skoog, I., 2005. High total cholesterol levels in late life associated with a reduced risk of dementia. Neurology 64, 1689–1695.
Miyake, A., Friedman, N.P., Emerson, M.J., Witzki, A.H., Howerter, A., Wager, T.D., 2000. The Unity and Diversity of executive functions and their contributions to complex "frontal lobe" tasks: a latent variable analysis. Cogn. Psychol. 41, 49–100.
Panchal, S.K., Brown, L., 2011. Rodent models for metabolic syndrome research. J. Biomed. Biotechnol. 2011, 351982. https://doi.org/10.1155/2011/351982.
Pistell, P.J., Morrison, C.D., Gupta, S., Knight, A.G., Keller, J.N., Ingram, D.K., Bruce-Keller, A.J., 2010. Cognitive impairment following high fat diet consumption is associated with brain inflammation. J. Neuroimmunol. 219, 25–32.
Ramos-Rodriguez, J.J., Jimenez-Palomares, M., Murillo-Carretero, M.I., Infante-Garcia, C., Berrocoso, E., Hernandez-Pacho, F., Lechuga-Sancho, A.M., Cozar-Castellano, I., Garcia-Alloza, M., 2015. Central vascular disease and exacerbated pathology in a mixed model of type 2 diabetes and Alzheimer's disease. Psychoneuroendocrinology 62, 69–79.
Sabia, S., Nabi, H., Kivimaki, M., Shipley, M.J., Marmot, M.G., Singh-Manoux, A., 2009. Health behaviors from early to late midlife as predictors of cognitive function: the Whitehall II study. Am. J. Epidemiol. 170, 428–437.
Stuss, D.T., Alexander, M.P., 2000. Executive functions and the frontal lobes: a conceptual view. Psychol. Res. 63, 289–298.
Sunyer, B., Patil, S., Frischer, C., Höger, H., Selcher, J., Brannath, W., Lubec, G., 2007. Strain-dependent effects of SGS742 in the mouse. Behav. Brain Res. 181, 64–75.
Tesauro, M., Cardillo, C., 2011. Obesity, blood vessels and metabolic syndrome. Acta Physiol (Oxford) 203, 279–286.
Toth, P., Szarka, N., Farkas, E., Ezer, E., Czeiter, E., Amrein, K., Ungvari, Z., Hartings, J.A., Buki, A., Koller, A., 2016. Traumatic brain injury-induced autoregulatory dysfunction and spreading depression-related neurovascular uncoupling: Pathomechanisms, perspectives, and therapeutic implications. Am. J. Physiol. Heart Circ. Physiol. 311, H1118–H1131.
Toyama, K., Koibuchi, N., Hasegawa, Y., Uekawa, K., Yasuda, O., Sueta, D., Nakagawa, T., Ma, M., Kusaka, H., Lin, B., Ogawa, H., Ichijo, Hidenori, Ichijo, Hidenor, Kim-Mitsuyama, S., 2015. ASK1 is involved in cognitive impairment caused by long-term high-fat diet feeding in mice. Sci. Rep. 5, 10844.
Tümer, N., Toklu, H.Z., Muller-Delp, J.M., Oktay, Ş., Ghosh, P., Strang, K., Delp, M.D., Scarpace, P.J., 2014. The effects of aging on the functional and structural properties of the rat basilar artery. Phys. Rep. 2, e12031.
Valcarcel-Ares, M.N., Tucsek, Z., Kiss, T., Giles, C.B., Tarantini, S., Yabluchanskiy, A., Balasubramanian, P., Gautam, T., Galvan, V., Ballabh, P., Richardson, A., Freeman, W.M., Wren, J.D., Deak, F., Ungvari, Z., Csiszar, A., 2019. Obesity in aging exacerbates Neuroinflammation, Dysregulating synaptic function-related genes and altering eicosanoid synthesis in the mouse Hippocampus: potential role in impaired synaptic plasticity and cognitive decline. J. Gerontol. A Biol. Sci. Med. Sci. 74, 290–298.
Valenti, R., Charidimou, A., Xiong, L., Boulouis, G., Fotiadis, P., Ayres, A., Riley, G., Kuijf, H.J., Reijmer, Y.D., Pantoni, L., Gurol, M.E., Davidsdottir, S., Greenberg, S.M., Viswanathan, A., 2017. Visuospatial functioning in cerebral amyloid Angiopathy: a pilot study. J. Alzheimers Dis. 56, 1223–1227.
van Dijk, G., van Heijningen, S., Reijne, A.C., Nyakas, C., van der Zee, E.A., Eisel, U.L.M., 2015. Integrative neurobiology of metabolic diseases, neuroinflammation, and neurodegeneration. Front. Neurosci. 9, 173.
Vuoksimaa, E., Rinne, J.O., Lindgren, N., Heikkilä, K., Koskenvuo, M., Kaprio, J., 2016. Middle age self-report risk score predicts cognitive functioning and dementia in 20–40 years. Alzheimer's & Dement. 4, 118–125.
Wang, C., Tao, Q., Wang, Xinghe, Wang, Xiurong, Zhang, X., 2016. Impact of high-fat diet on liver genes expression profiles in mice model of nonalcoholic fatty liver disease. Environ. Toxicol. Pharmacol. 45, 52–62.
Wang, Q., Yuan, J., Yu, Z., Lin, L., Jiang, Y., Cao, Z., Zhuang, P., Whalen, M.J., Song, B., Wang, X.-J., Li, X., Lo, E.H., Xu, Y., Wang, X., 2018. FGF21 attenuates high-fat diet-induced cognitive impairment via metabolic regulation and anti-inflammation of obese mice. Mol. Neurobiol. 55, 4702–4717.
Whitmer, R.A., Sidney, S., Selby, J., Johnston, S.C., Yaffe, K., 2005. Midlife cardiovascular risk factors and risk of dementia in late life. Neurology 64, 277–281.
Winters, B.D., Saksida, L.M., Bussey, T.J., 2008. Object recognition memory: neurobiological mechanisms of encoding, consolidation and retrieval. Neurosci. Biobehav. Rev. 32, 1055–1070.
Wolk, D.A., Signoff, E.D., DeKosky, S.T., 2008. Recollection and familiarity in amnestic mild cognitive impairment: a global decline in recognition memory. In: Neuropsychologia, Part Special Issue: What Is the Parietal Lobe Contribution to Human Memory? vol. 46. pp. 1965–1978.
Wong, S.K., Chin, K.-Y., Suhaimi, F.H., Fairus, A., Ima-Nirwana, S., 2016. Animal models of metabolic syndrome: a review. Nutr. Metab. (Lond.) 13.
Zhou, B., Nakatani, E., Teramukai, S., Nagai, Y., Fukushima, M., Alzheimer's Disease Neuroimaging Initiative, 2012. Risk classification in mild cognitive impairment patients for developing Alzheimer's disease. J. Alzheimers Dis. 30, 367–375.